International Journal of Modern Physics A Vol. 35, Nos. 11 & 12 (2020) 2030006 (39 pages) © World Scientific Publishing Company



 $DOI:\,10.1142/S0217751X20300069$ 

### Frontiers in lattice nucleon structure

#### Huey-Wen Lin

Department of Physics and Astronomy, and Computational Mathematics, Science & Engineering, Michigan State University, East Lansing, MI 48824, USA hwlin@pa.msu.edu

> Received 1 January 2020 Accepted 27 March 2020 Published 11 May 2020

In this paper, I review recent progress in lattice-QCD calculations of hadron structure with an emphasis on nucleon structure. A wide range of nucleon observables are being studied in modern lattice calculations, and important progress has been made at physical pion mass, including the spin decomposition of the nucleon and the Bjorken-x dependence of hadron structure. Challenges and perspectives for future lattice hadron-structure calculations will be discussed.

Keywords: Lattice field theory; quantum chromodynamics; nucleon structure; proton spin.

PACS numbers: 12.38.Gc, 14.20.Dh, 13.60.Hb

#### 1. Introduction

Nucleons (that is, protons and neutrons) are the building blocks of all ordinary matter, and the study of nucleon structure is a critical part of the Department of Energy (DOE) mission. Gluons and quarks are the underlying degrees of freedom that explain the properties of nucleons, and fully understanding how they contribute to the properties of nucleons (such as their mass or spin structure) helps to decode the Standard Model that rules our physical world. In the theory of quantum chromodynamics (QCD), a branch of the Standard Model, gluons strongly interact with themselves and with quarks, binding both nucleons and nuclei. However, due to their confinement within these bound states, we cannot single out individual gluons to study them, and the predicted state that is made up of these particles only has yet to be experimentally observed. Many mysteries remain after decades of experimental effort; for example, what is the origin of the proton mass? How are sea quarks and gluons, and their spins, distributed in space and momentum inside the nucleon? Therefore, the exploration of the nucleus continues: in the US, physics targets are being pursued by multiple DOE laboratories, Brookhaven

National Laboratory (BNL) and JLab, as well as the future Electron-Ion Collider (EIC). Worldwide, facilities such as Gesellschaft für Schwerionenforschung (GSI) in Germany and Japan Proton Accelerator Research Complex (J-PARC) in Japan will join the effort, and future facilities are being considered, such as an EIC machine in China and the Large Hadron-Electron Collider (LHeC) at CERN.

Lattice QCD is an ideal theoretical tool to study the parton structure of hadrons, starting from quark and gluon degrees of freedom. LQCD is a regularization of continuum QCD using a discretized four-dimensional spacetime; it contains a small number of natural parameters, such as the strong coupling constant and quark masses. Unlike continuum QCD, LQCD works in Euclidean spacetime (rather than Minkowski), and the coupling and quark masses can be set differently than those in our universe. The theory contains two scales that are absent in continuum QCD, one ultraviolet (the lattice spacing a) and one infrared (the spatial extent of the box L); this setup keeps the number of degrees of freedom finite so that LQCD can be solved on a computer. For observables that have a well-defined operator in the Euclidean path integral for numerical integration, we can find their values in continuum QCD by taking the limits  $a \to 0$ ,  $L \to \infty$  and  $m_q \to m_q^{\rm phys}$ . LQCD is a natural tool to study the structure of hadrons, since quarks and gluons are the fundamental degrees of freedom.

Progress has long been limited by computational resources, but recent advances in both algorithms and a worldwide investment in pursuing exascale computing has led to exciting progress in LQCD calculations. Take the nucleon tensor charge for example. Experimentally, one gets the tensor charges by taking the zeroth moment of the transversity distribution; however, the transversity distribution is poorly known and such a determination is not very accurate. On the lattice side, there are a number of calculations of  $g_T$ ;<sup>1–9</sup> some of them are done with more than one ensemble at physical pion mass with high-statistics calculations (about 100 k measurements) and some with multiple lattice spacings and volumes to control lattice artifacts. Such programs would have been impossible 5 years ago. As a result, the lattice-QCD tensor-charge calculation has the most precise determination of this quantity, which can then be used to constrain the transversity distribution and make predictions for upcoming experiments.<sup>10</sup> One can imagine that many of the quantities less known from experiments can greatly benefit from lattice-QCD predictions and constraints.

However, for decades, probing hadron structure with lattice QCD was limited to only the first few moments (integrals over the distributions), due to complications arising from the breaking of rotational symmetry by the discretized Euclidean spacetime. In principle, this problem can be avoided by working with moments of parton distributions, which correspond to matrix elements of local operators, provided all the moments can be computed to recover the whole PDF. In practice, one can only obtain the first few (about 3) moments due to operator mixing with lower-dimension operators with coefficients proportional to inverse powers of the lattice spacing, which divergent in the continuum limit. Even if one could design more

complicated operators to subtract the power divergence arising from the mixing of high-moment operators to get to even higher moments, the renormalization for the higher-moment operators becomes significantly more complicated, and the correlators suffer from signal-to-noise problems as well. Thus, in practice, most calculations in recent years were limited to the first couple moments. Higher moments, such as  $\langle x^2 \rangle$ , have not been updated using dynamical fermions for more than a decade. There are interesting proposals to obtain higher moments by using smeared sources to overcome the power-divergent mixing problem and by using light-quark—to-heavy-quark transition currents to compute current—current correlators in Euclidean space. There are also ideas about obtaining the structure functions directly from the hadronic tensor current. Hence the lattice numerical calculation.

The paper by X.-D. Ji<sup>18</sup> proposed a much more straightforward way of calculating the full x dependence of the distribution for PDFs and generalized parton distributions (GPDs) (and other quantities) without dealing with many moments nor requiring enormous computational resources to achieve. In this large-momentum effective theory (LaMET) framework, we take an operator containing an integral of gluonic field strength along a line and boost the nucleon momentum toward the speed of light, tilting the spacelike line segment toward the lightcone direction. The time-independent, nonlocal (in space) correlators at finite  $P_z$  can be directly evaluated on the lattice. For example, the quark unpolarized distribution can be calculated via

$$q_{\rm lat}(x,\mu,P_z) = \int \frac{dz}{4\pi} e^{izk} \times \langle \mathbf{P} | \bar{\psi}(z) \Gamma \left( \prod_n U_z(n\hat{z}) \right) \psi(0) | \mathbf{P} \rangle, \qquad (1)$$

where  $U_z$  is a discrete gauge link in the z direction,  $x=k/P_z$ ,  $\mu$  is the renormalization scale and  ${\bf P}$  is the momentum of the hadron, taken such that  $P_z \to \infty$ . The matrix  $\Gamma$  fixes the type of parton distribution, e.g.  $\Gamma = \gamma_z$ ,  $\gamma_t$  corresponds to unpolarized parton distribution, while for helicity and transversity distributions one has  $\Gamma = i\gamma_5\gamma_z$  and  $\Gamma = i\gamma_5\gamma_x\gamma_z$ , respectively. Since no amount of boost will take the nucleon exactly onto the lightcone, there remain corrections power-suppressed by  $P_z$  as  $O\left(M_H^2/P_z^2, \Lambda_{\rm QCD}^2/P_z^2\right)$  (where  $M_H$  is hadron mass). The same idea can be straightforwardly applied to helicity  $\Delta q(x,\mu)$  and transversity  $\delta q(x,\mu)$  for the direct lattice-QCD calculation of these quantities.

The first attempt to apply the LaMET approach to compute parton observables was the calculation of the unpolarized isovector quark distribution, <sup>19,24,25</sup> and this work was closely followed by ETMC (a European lattice group). <sup>20</sup> Similarly, when the helicity and transversity distributions were computed, <sup>21</sup> an ETMC follow-up work soon appeared. <sup>26</sup> Such interest shows that this new research field is very active and competitive. Although currently, lattice systematics are not yet fully accounted for, a sea-flavor asymmetry has been qualitatively seen in both the unpolarized and linearly polarized cases, part of which has been confirmed in the updated measurements by the STAR and PHENIX collaborations. The Drell–Yan

experiments at FNAL (E1027+E1039) and future EIC data will be able to give more insight into the sea asymmetry in the transversely polarized nucleon.

The rest of the review is organized as follows. I will briefly introduce lattice QCD and bring the readers up-to-speed on how to read lattice numbers and their corresponding uncertainties in Sec. 2. In Sec. 3, I will highlight a few nucleon structure studies with fully controlled systematics. In Sec. 4, I will mention a few examples of recent attempts to determine the Bjorken-x dependence of structure. A summary and future outlook can be found in Sec. 5.

## 2. Lattice-QCD 101

Lattice QCD (LQCD) is a theoretical tool that allows us to study QCD directly with full systematic control. The approach is based on regularizing QCD on a finite Euclidean lattice, and is often studied in the nonperturbative regime using numerical computations on national-scale supercomputers. QCD correlation functions in the path-integral formalism<sup>27–30</sup> are calculated using methods adapted from statistical mechanics. To make contact with experimental data, the numerical results are extrapolated to the continuum (with lattice spacing  $a \to 0$ ) and infinite-volume  $(L \to \infty)$  limits. When the calculation is done using heavier-than-physical quark masses (to save computational time), one also has to take the  $m_q \to m_q^{\rm phys}$  limit. In the past decade, there has been significant progress in the development of efficient algorithms for the generation of ensembles of gauge-field configurations and tools for extracting relevant information from lattice-QCD correlation functions. Lattice-QCD calculations have reached a level where they not only complement, but also guide current and forthcoming experimental programs.  $^{33,34}$ 

Lattice-QCD calculations must demonstrate control over all sources of systematic uncertainty introduced by the discretization of QCD on the lattice to make meaningful comparisons with experimental data or provide predictions for physical world. These include discretization effects from nonzero lattice spacing, extrapolation from unphysically heavy pion masses, finite-volume effects, and renormalization of composite operators. We briefly review these main sources of systematic uncertainty here; see Ref. 35 for a detailed discussion by FLAG (Flavor Lattice Averaging Group), focusing on mesonic quantities. A similar standard was first applied to lattice nucleon structure by Precision Neutron-Decay Matrix Elements (PNDME) collaboration<sup>3,4</sup> with extension to excited-state systematics, which are more significant for the nucleon case. These extensions were later adapted by a topical review<sup>36</sup> and are now included in latest FLAG Review in 2019.<sup>37</sup>

• Discretization effects and the continuum limit. Discretization introduces an additional parameter to QCD, the lattice spacing a; however, this also allows a fair degree of flexibility in discretizing the QCD action, which has led to a variety of formulations. For the gluon action, one can easily construct operators that are  $O(a^2)$ -improved without increasing the computational cost much. However, to improve the fermion action beyond the simplest discretizations at O(a) increases

the computational cost by huge amounts. Since this would be the leading systematic relative to the gluon action, lattice discretization effects are often classified by the type of fermion action used for the quarks. In practice, one cannot afford to perform numerical simulations at arbitrarily small lattice spacings, because the cost of computation increases with a large inverse power of the lattice spacing. Thus, O(a) effects can remain significant even with current lattice spacings ranging from 0.15 fm to 0.05 fm.

- Pion-mass dependence. The computational cost to evaluate the fermion contribution to the path integral increases with a large inverse power of the quark mass (or equivalently, the pion mass). Therefore, lattice-QCD calculations are often performed at unphysically heavy pion masses. In recent years, with the help of hardware and software advancements, there are increasingly many results published using direct calculation at the physical pion masses. However, such direct calculations at the physical quark masses still yield larger statistical uncertainty. To obtain better results at the physical pion mass, lattice data are generated over a range of pion masses and then extrapolated to the physical pion mass. To control the associated systematic uncertainties, these extrapolations are guided by effective theories. In particular, the pion-mass dependence can be parametrized using chiral perturbation theory (XPT), 38 which accounts for the Nambu–Goldstone nature of the lowest excitations that occur in the presence of light quarks. However, XPT does not work well in nucleon studies, so people often study multiple pion-mass dependences and report combined-analysis systematics. 10,39
- Finite-volume effects. Numerical lattice-QCD calculations are necessarily restricted to a finite spacetime volume, e.g. a hypercube of side L. For most simple quantities, these effects decay exponentially with the size of the lattice,  $^{40,41}$  and therefore the easiest way to minimize or eliminate finite-volume effects is to choose the volume sufficiently large in physical units. Unfortunately, this can be prohibitively expensive as one approaches the continuum limit, requiring the number of lattice sites to grow as L/a in all four dimensions. In general, finite-volume effects of hadrons are dominated by their interactions with pions; numerical evidence suggests that lattice sizes of  $m_{\pi}L \geq 4$ , where  $m_{\pi}$  is the pion mass, are generally sufficiently large that finite-volume effects are negligible for mesons, within the current precision of lattice-QCD calculations. From the studies of the pseudoscalar and electromagnetic form factors of the nucleon, it is evident that larger physical volumes are sometimes needed for the baryons. One must study this case by case.
- Excited-state contamination. A lattice-QCD correlation function can be decomposed into a sum over a tower of states whose contributions behave like  $e^{-E_i t}$ , where  $E_i$  is the energy of the *i*th state and *t* is Euclidean time. Thus, at large Euclidean times, ground-state quantities can be extracted by fitting to the dominant exponential behavior. Unfortunately, the signal-to-noise ratio is exponentially suppressed with Euclidean time; for nucleon quantities it goes like  $e^{-(E_N-3M_\pi/2)t}$ , where  $E_N$  is the nucleon energy,<sup>42</sup> and similarly for any

state of interest heavier than the pseudoscalar mesons. Thus, most lattice-QCD results must be extracted from an intermediate region in which excited-state contributions are either small or well-controlled and the signal-to-noise ratio is sufficiently large that the signal can be reliably extracted. This is a particular challenge for baryons and is one of the largest sources of systematic uncertainty for nucleon matrix elements. There were multiple early studies<sup>43–46</sup> advocating for excited-state contamination to be included in nucleon analysis, but only recently has it become common practice.

• Renormalization. The matrix elements extracted from a lattice-QCD calculation at a given lattice spacing are "bare" matrix elements, rendered finite by the presence of the lattice spacing, which serves as a gauge-invariant UV regulator. Therefore, the result is lattice spacing dependent. One must renormalize the operators and fields to remove the regulator dependence and match them to some common scheme and scale used by phenomenologists after taking the continuum limit. Although renormalization is traditionally discussed in the framework of perturbation theory, at hadronic energy scales the renormalization constants should be computed nonperturbatively to avoid uncontrolled uncertainties due to truncated perturbative results. This requires a renormalization condition that can be implemented on the lattice and in continuum perturbation theory. In QCD with only light quarks, it is technically advantageous to employ mass-independent renormalization schemes. A common choice is the regularization-independent/ momentum (RI/MOM) scheme. 47 Finally, to compare with experiments, which often use the minimal-subtraction  $(\overline{MS})$  scheme, a conversion factor from the nonperturbative scheme must be computed perturbatively.

In addition, on a hypercubic lattice, the orthogonal group O(4) of continuum Euclidean spacetime is reduced to the hypercubic group H(4). Thus, operators are classified according to irreducible representations of H(4).<sup>48</sup> Different irreducible representations belonging to the same O(4) multiplet will, in general, give different answers at finite lattice spacing, an effect that can be reduced by improving the operators.<sup>11</sup> Conversely, operators that lie in different irreducible representations of O(4), but the same irreducible representations of H(4), will mix at finite lattice spacing but not in the continuum. When these operators have lower mass dimensions, the mixing coefficients scale with the inverse lattice spacing to some power, and diverge in the continuum limit. This power-divergent mixing must be removed nonperturbatively, and is a particular challenge for lattice calculations of the Mellin  $n \leq 3$  moments of PDFs.

To illustrate what needs to be done to obtain reliable nucleon observables from lattice QCD, examples from recent PNDME's calculation of nucleon charges are shown in Fig. 1.<sup>1</sup> To reach the continuum limit  $(a \to 0)$ , at the physical pion mass  $(M_{\pi} \approx 135 \text{ MeV})$  and in the infinite-volume limit  $(L \to \infty)$ , physics motivated fit ansatz is used. To parametrize the dependence on  $M_{\pi}$  and the finite-volume parameter  $M_{\pi}L$ , we report results from finite-volume chiral perturbation

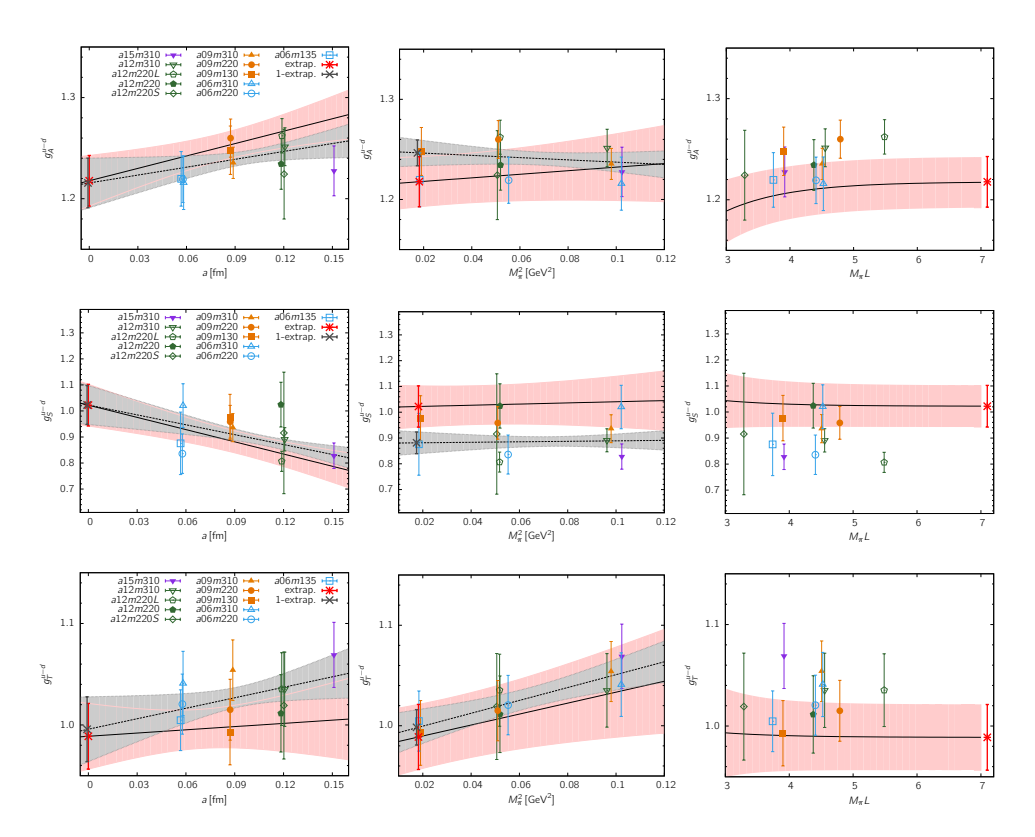


Fig. 1. (Color online) The continuum-extrapolated renormalized isovector charges  $g_A^{u-d}$ ,  $g_S^{u-d}$ , and  $g_T^{u-d}$  in the  $\overline{\rm MS}$  scheme at 2 GeV using Eq. (2). The result of the simultaneous extrapolation to the physical point defined by  $a \to 0$ ,  $M_\pi \to M_\pi^{\rm phys} \approx 135$  MeV and  $M_\pi L \to \infty$  is marked by a red star. The pink error band in each panel is the result of the simultaneous fit but shown as a function of a single variable. The overlay in the left (middle) panels with the dashed line within the gray band is the fit to the data versus a ( $M_\pi^2$ ), i.e. neglecting dependence on the other two variables. The symbols used to plot the data are defined in the left panels. These plots are taken from Ref. 1.

theory.  $^{49-55}$  For the lattice discretization effects, the corrections start with the term linear in a since the action and the operators in our clover-on-HISQ formalism are not fully O(a) improved. Keeping just the leading correction term in each, plus possibly the chiral logarithm term discussed below, our approach is to make a simultaneous fit in the three variables to the data from the eleven ensembles. For the isovector charges and the flavor diagonal axial and tensor charges, the ansatz is

$$g_{A,S,T}^{u-d}(a, M_{\pi}, L) = c_1 + c_2 a + c_3 M_{\pi}^2 + c_3 M_{\pi}^2 \ln \left(\frac{M_{\pi}}{M_{\rho}}\right)^2 + c_4 M_{\pi}^2 \frac{e^{-M_{\pi}L}}{X(M_{\pi}L)},$$
(2)

where  $M_{\rho}$  in the chiral logarithm is the renormalization scale.

Table 1. (Color online) A summary of the control over various sources of systematic errors in lattice-QCD calculations of the isovector tensor charge  $g_T^{u-d}$  using the FLAG quality criteria.<sup>35</sup> Note that the errors in the table are quoted from papers which often only contain quark-mass extrapolations, not the continuum  $a \to 0$  extrapolation (except for PNDME). In order to use a quantity as a SM input, it is important to have green-star rating for each potential systematic uncertainty to make sure all lattice artifacts under control.

	Refs. $P_{\rm ublication}$ $S_{\rm tatus}$				Chiral Extrapolation Extrapolation Chiral Continuum Extrapolation Einite Excited State Renormalization 9T					
Collaboration	Refs.	Raj	$N_f$	Chir	Con	Fini	Exc	Ren	$g_T$	
PNDME'16	3	A	2 + 1 + 1	*	*	*	*	*	0.987(51)(20)	
PNDME'15	4	A	2 + 1 + 1	*	*	*	*	*	1.020(76)	
ETMC'15	7	$^{\rm C}$	2 + 1 + 1			*	*	*	1.053(21)	
LHPC'12	5	A	2 + 1	*	0	*	0	*	1.038(11)(12)	
${\rm RBC/UKQCD'10}$	6	A	2+1	0		*		*	0.9(2)	
RQCD'14	8	A	2	*	*	*	0	*	1.005(17)(29)	
ETMC'15	7	A	2	*			*	*	1.027(62)	
RBC'08	58	A	2			*		*	0.93(6)	

We use the recent LQCD calculation of the isovector tensor charge as a demonstration of the standards one should apply to all nucleon matrix elements calculations. To use LQCD numbers to replace Standard Model inputs, we must be absolutely sure that all sources of systematic uncertainty (quark mass,  $a \to 0$ ,  $V \to \infty$ ) are controlled. Table 1 shows a summary of the level of control over various systematics in the calculation of the nucleon isovector tensor charge using simulations of lattice QCD with  $N_f = 2$ , 2 + 1 and 2 + 1 + 1 flavors<sup>a</sup> in the FLAG format. <sup>35,56,57</sup> Note that a community-wide consensus on applying the FLAG criteria to matrix elements of nucleon states does not yet exist. However, the level of uncertainty is of particular concern, since there is no firm experimental measurement of the tensor charge. Therefore, it is important for LQCD to quote the full errors.

In the case of the nucleon, we need to include a systematic for excited-state contamination, since it has been shown in many works that it can significantly change the final results. Here is our notation:

### • Publication status:

- A published or minor update of published results
- P preprint
- C conference contribution

<sup>&</sup>lt;sup>a</sup>This indicates the number of species of quark in the QCD vacuum; 2 being degenerate up/down quarks, 2+1 has additional strange degrees of freedom, and 2+1+1 has up/down, strange and charm loops in the QCD vacuum.

- Chiral extrapolation:
  - $\star M_{\pi, \min} < 200 \text{ MeV}$
  - $\circ$  200 MeV  $\leq M_{\pi, \min} \leq 400$  MeV
  - $\blacksquare$  400 MeV  $< M_{\pi, \min}$
- Finite-volume effects:
  - ★  $M_{\pi,\min}L > 4$  or at least 3 volumes
  - O  $M_{\pi,\min}L > 3$  and at least 2 volumes
- Renormalization:
  - \* nonperturbative
  - $\circ$  1-loop perturbation theory or higher with a reasonable estimate of truncation errors
- Continuum extrapolation:
  - ★ 3 or more lattice spacings, at least 2 points below 0.1 fm
  - $\circ$  2 or more lattice spacings, at least 1 point below 0.1 fm
- Excited states:
  - ★  $t_{\rm sep,\,max} > 1.5$  fm or at least 3 source-sink separations  $t_{\rm sep}$  investigated at each lattice spacing and at each  $M_{\pi}$ .
  - $\circ$  At least 2 source-sink separations with 1.2 fm  $\leq t_{\rm sep,\,max} \leq 1.5$  fm and at least one  $M_{\pi}$  at each lattice spacing.

For the last 4 items, criteria not meeting listed standards would be labeled  $\blacksquare$ . Plots of the global lattice data, as summarized in Table 1, along with phenomenological estimates of  $g_T$  are shown in middle panel of Fig. 2. The nucleon tensor charge is one of the least known nucleon couplings and many ongoing and planned experiments will narrow down its value. For reliable lattice-QCD predictions, such as those we plan in this proposal, it is crucial to have all systematics under control (as marked with a green star in each systematic rating) so that lattice artifacts will

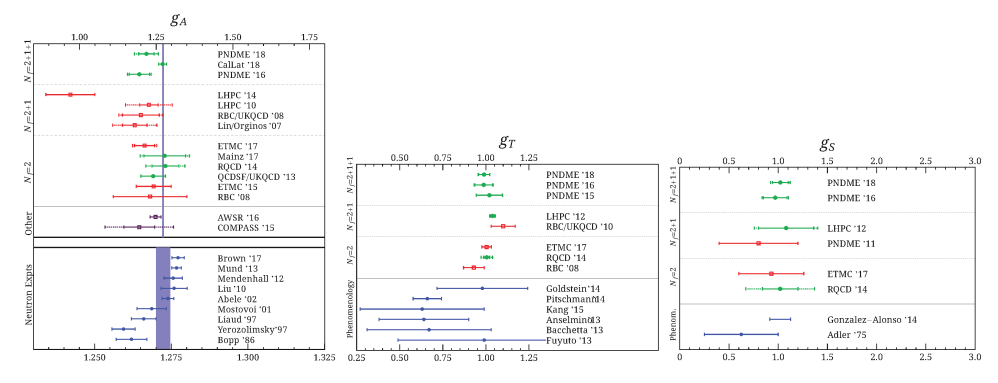


Fig. 2. (Color online) A summary of results for the isovector axial charge  $g_A^{u-d}$  (left), tensor charge  $g_T^{u-d}$  (middle) and scalar charge  $g_S^{u-d}$  (right), for  $N_f=2$ , 2+1- and 2+1+1 flavors. The lattice and phenomenological results quoted can be found in Ref. 1. The lattice-QCD estimates in red indicate that estimates of excited-state contamination, or discretization errors, or chiral extrapolation were not presented. When available, systematic errors have been added to statistical ones as outer error bars marked with dashed lines.

away.

be reliably constraining the nucleon structure or inputs toward the final determinations on the impact to nuclear physics. Similar ratings for nucleon isovector axial and scalar charges are also applied and shown in Fig. 2. Note that a similar rating idea has been adapted and modified in the joint-community white paper<sup>36</sup> with criteria determined by representatives from the worldwide lattice nucleon-structure collaborations.

# 3. Nucleon Structure in the Continuum Limit

In this section, we discuss selected recent results and examples of lattice-QCD nucleon structure with the continuum limit taken. We also discuss the impacts of these results on phenomenology.

Improving Nucleon Transverse Structure with Lattice Tensor Charges:

## 3.1. Precision nucleon tensor charges and their applications

The transverse momentum distributions (TMDs) provide important information in mapping out nucleon structure in the transverse plane and are one of the big remaining unsolved QCD puzzles. The universality of the Collins form factors (FFs)<sup>59</sup> allows different types of experimental processes to be combined in global QCD analyses. Several previous studies<sup>60–64</sup> have used semi-inclusive deep inelastic scattering (SIDIS) and  $e^+e^-$  annihilation measurements to extract the TMDs. Anselmino et al.  $^{60-62}$  used a factorized ansatz to relate the TMDs to the transversity  $h_1^q$  PDFs and Gaussian transverse momentum widths, while Kang et al. 63,64 parametrized the  $h_1^q$  PDF in terms of the unpolarized and helicity distributions and embedded this inside the Collins-Soper-Sterman (CSS) evolution formalism. <sup>65</sup> Working within the collinear factorization framework, Bacchetta et al. 66,67 also extracted transversity PDFs from pion-pair production in SIDIS using dihadron FFs from  $e^+e^-$  annihilation data. The results of these analyses were generally compatible, giving values for the isovector moment  $g_T \equiv \delta u - \delta d$  in the range 0.5–1 with sizable, 30–50%, uncertainties. Note that in all these studies, the experimental coverage is restricted to the region  $0.02 \lesssim x \lesssim 0.3$ , so that the determination of the full moment  $g_T = \int dx \, h_1^q(x)$ relies largely on extrapolation outside the measured region. Additional data from

Reference 10 sees the opportunity to use lattice tensor data to provide constraints where experimental data is limited. Using three available lattice  $g_T$  works that use multiple lattice spacings, volumes and quark masses to control all possible systematics on the lattice,  $^{3,5,8}$  we perform a continuum-limit extrapolation of  $g_T$  using all possible combinations of the leading terms for the fitting formulas associated with these lattices. Combining these fits using the Akaike information criterion then yields  $g_T^{\text{lat}} = 1.008(56)$ . We then use the lattice  $g_T$  to constrain the global-analysis fits to SIDIS  $\pi^{\pm}$  production data from proton and deuteron targets, including their x, z and  $P_{h,\perp}$  dependence, with a total of 176 data points collected from measurements at HERMES<sup>68</sup> and COMPASS.  $^{69,70}$  This gives in principle 8

future experiments will help constrain the transversity, but they are a few years

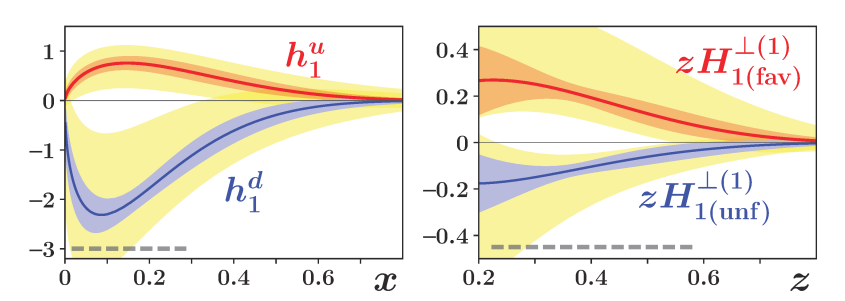


Fig. 3. Up- (left) and down-quark (right) transversity distributions using SIDIS data with and without lattice  $g_T$  constraints.<sup>10</sup> This is one demonstration of how the combination of experiment and precision lattice-moment inputs can greatly advance our knowledge of nucleon structure. These plots are taken from Ref. 10.

linear combinations of transversity TMD PDFs and Collins TMD FFs for different quark flavors, from which we attempt to extract the u and d transversity PDFs and the unfavored Collins FFs, together with their respective transverse-momentum widths. In Fig. 3 we see the lattice-QCD  $g_T$ , zeroth moment of the transversity distribution, has made a significant impact and makes a clear improvement in the constraint over a wide range of x. As more precision moments become available, the improvement in transversity, one of the TMD functions, will be more significant. The direct calculation of the x dependence of structure functions will provide a better picture and direct constraints in the large-x regions. With an improved determination of the transversity, one can use the future Jefferson-Lab transversity data to better understand the poorly known fragmentation functions, and enhance the discovery capabilities of the TMD program.

Constraining New-Physics Scenarios Using Precision Beta-Decay Measurements and Lattice Charges: Searches for new physics are ongoing from the high-energy frontier, such as at the largest machine ever built by mankind, the Large Hadron Collider (LHC), to low-energy precision experiments, such as nucleon beta decay. Loop effects and new interactions at the TeV scale can generate effective scalar or tensor interactions at the hadronic scale that are not present in the Standard Model and can be probed in neutron decays or at the TeV scale directly at the LHC. At low energy, such scalar and tensor interactions contribute to the helicity-flip parameters b and  $b_{\nu}$  in the neutron-decay distribution.<sup>71</sup> Thus, one can put constraints on novel scalar and tensor interactions at the TeV scale as described in Ref. 71, by combining the precision lattice calculation of the scalar and tensor charges with the measurements of b and  $b_{\nu}$  in low-energy experiments. To optimally bound such scalar and tensor interactions using measurements of band  $b_{\nu}$  parameters in planned experiments targeting 10<sup>-3</sup> precision,<sup>72</sup> the level of precision required in  $g_S^{u-d}$  and  $g_T^{u-d}$  is at the 10% level, as explained in Refs. 71 and 72. The lattice calculations of  $g_T^{u-d}$  are currently more precise than moments from the globally fitted transversity, and the only direct way of accessing  $g_S^{u-d}$  is

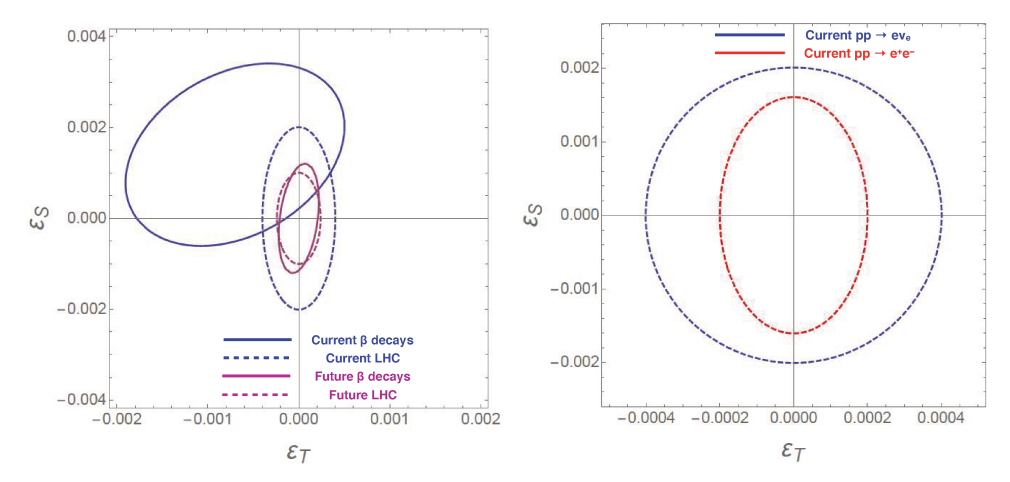


Fig. 4. (Left) Current and projected 90% CL constraints on  $\epsilon_S$  and  $\epsilon_T$  defined at 2 GeV in the  $\overline{\rm MS}$  scheme from Ref. 1. (Right) Comparison of current LHC bounds from  $pp \to e + {\rm MET} + X$  versus  $pp \to e^+e^- + X.^1$ 

through lattice QCD. Therefore, lattice inputs are critical to these planned  $10^{-3}$  precision low-energy experiments.

New physics due to nonstandard scalar and tensor charged-current interactions can be parametrized by the dimensionless couplings  $\epsilon_{S,T}$ , which are inversely proportional to the new-physics scales  $\Lambda_{S,T}^{-2}$ :1,71,73

$$\mathcal{L}_{CC} = -\frac{G_F^{(0)} V_{ud}}{\sqrt{2}} \left[ \epsilon_S \bar{e} (1 - \gamma_5) \nu_\ell \cdot \bar{u} d + \epsilon_T \bar{e} \sigma_{\mu\nu} (1 - \gamma_5) \nu_\ell \cdot \bar{u} \sigma^{\mu\nu} (1 - \gamma_5) d \right]. \tag{3}$$

These couplings can be constrained by a combination of low-energy precision betadecay measurements (of the pion, neutron, and nuclei) combined with our results for the isovector charges  $g_S^{u-d}$  and  $g_T^{u-d}$ , as well at the LHC through the reaction  $pp \to 0$  $e\nu + X$  and  $pp \to e^+e^- + X$ . The LHC constraint is valid provided the mediator of the new interaction is heavier than a few TeV. The left-hand side of Fig. 4 shows current and projected bounds on  $\{\epsilon_S, \epsilon_T\}$  defined at 2 GeV in the  $\overline{\text{MS}}$  scheme. The experimental beta-decay constraints are taken from the review article in Ref. 74. The current analysis includes all existing neutron and nuclear-decay measurements, while the future projection assumes measurements of the various decay correlations with fractional uncertainty of 0.1%, the Fierz interference term at the  $10^{-3}$  level, and neutron lifetime with uncertainty  $\delta \tau_n = 0.1$  s. The current LHC bounds are obtained from the analysis of the  $pp \rightarrow e + \text{MET} + X$ , where MET stands for missing transverse energy from the ATLAS results<sup>75</sup> at  $\sqrt{s} = 13$  TeV and integrated luminosity of 36 fb<sup>-1</sup>. The strongest bound comes by the cumulative distribution with a cut on the transverse mass at 2 TeV. The projected future LHC bounds are obtained by assuming that no events are observed at transverse mass greater than 3 TeV with an integrated luminosity of 300 fb<sup>-1</sup>. The LHC bounds become tighter on the inclusion of the Z-like mediated process  $pp \to e^+e^- + X$ . As shown in the right-hand side of Fig. 4, which includes both W-like and Z-like mediated processes, the current LHC bounds are comparable to future low-energy ones, motivating more precise low-energy experiments. The current analysis neglected the next-to-leading order (NLO) QCD corrections,  $^{76}$  which would further strengthen the LHC bounds by O(10%). Similar bounds are obtained using the Compact Muon Solenoid (CMS) data.  $^{77,78}$ 

# 3.2. Nucleon form factors

**Nucleon isovector axial form factors:** For neutrino physics, a key input from the SM would be the nucleon axial form factors  $(G_A)$  defined in terms of the isovector axial current

$$\langle N(p_f)|A^+_{\mu}(x)|N(p_i)\rangle = \bar{u}_N \left[\gamma_{\mu}\gamma_5 G_A(q^2) + iq_{\mu}\gamma_5 G_P(q^2)\right] u_N e^{iq \cdot x}. \tag{4}$$

Here,  $q=p_f-p_i$  is the momentum transfer between the initial and final state of nucleon; and the isovector current is  $A^+_{\mu}(x)=\bar{u}\gamma_{\mu}\gamma_5 u-\bar{d}\gamma_{\mu}\gamma_5 d$ .  $G_A(q^2)$  and  $G_P(q^2)$  are known as nucleon axial and induced-pseudoscalar form factors, and  $\bar{u}_N$  and  $u_N$  are the associated nucleon spinors. In the limit  $|\mathbf{q}| \to 0$ ,  $G_A(q^2=0)$  should recover the nucleon axial charge  $g_A=-1.2723(23)$ , which is well determined from neutron  $\beta$ -decay experiments. To Contrariwise, the axial-charge radius squared  $r_A^2$  is less known; once  $G_A(q^2)$  is obtained, one can obtain the radius via

$$r_A^2 \equiv \frac{6}{G_A(0)} \left. \frac{dG_A}{dq^2} \right|_{q^2=0}$$
 (5)

Although the first lattice-QCD calculation of the isovector nucleon axial form factors can be traced back to the early '90s, there has been significant progress and improvement by the global lattice community. One of the systematics, excited-state contamination, was not consistently addressed 10 years ago, which resulted in a lower nucleon axial coupling  $g_A$  and the wrong form factors. Removing this systematic has become a must-have for any lattice-QCD nucleon calculation. Another exciting breakthrough in the past decade is the increasing number of lattice nucleon calculations at the physical pion mass, thanks to recent advances in both algorithms and a worldwide investment in pursuing the first exascale computing machine. Many calculations now comes with high statistics (0(100 k) measurements) and some with multiple lattice spacings and volumes to control lattice artifacts. Such programs would have been impossible 5 years ago.

Figure 5 gives a summary of the recent nucleon axial form factors done near the physical pion mass. Among those, PNDME collaboration performed the most extensive study of the axial form factor: they use eight different 2+1+1-flavor HISQ ensembles generated by MILC collaboration<sup>80,81</sup> with lattice spacings in the range 0.06–1.2 fm and pion mass in the range 130–310 MeV; excited-state contamination is controlled via a three-state fit. Furthermore, PNDME's work includes more than one physical pion mass ensemble. The resulting axial form factor is not as steep as experimental determinations with  $m_A \approx 1 \text{ GeV}$ ; <sup>82</sup> however, it is compatible with MiniBooNE's  $m_A \approx 1.35 \text{ GeV}$ .

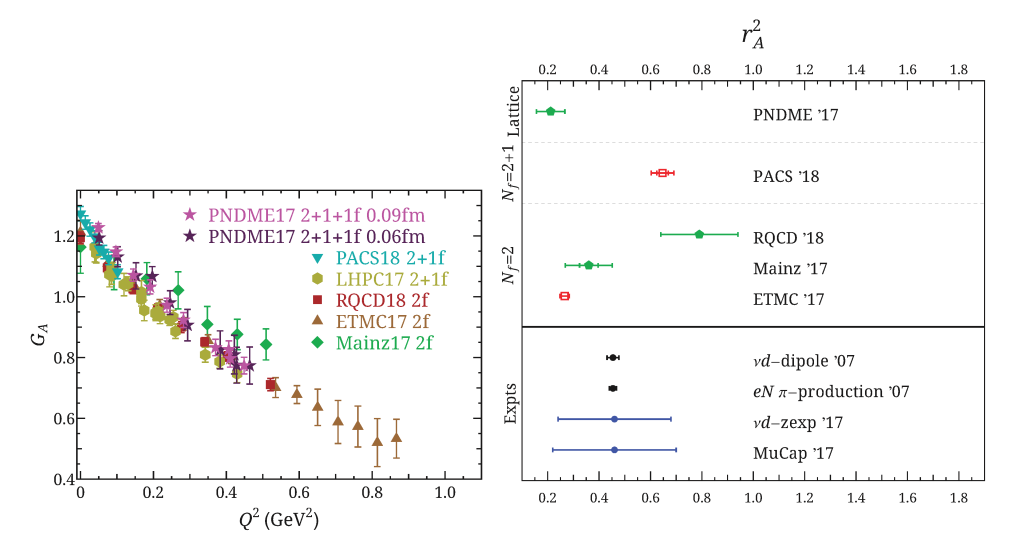


Fig. 5. (Color online) The nucleon isovector axial (left) form factors as functions of  $q^2$ , and a summary of  $r_A^2$  (right) from calculations involving ensembles near physical pion mass,<sup>87–92</sup> together with nonlattice determinations. The color code for  $r_A^2$  is adapted from the Flavor Lattice Averaging Group,<sup>35</sup> as specified in the Appendix of Ref. 4. The legends and references for  $r_A^2$  are as follows:  $\nu d$  (dipole) and  $eN \to eN'\pi$ ,<sup>93</sup>  $\nu d$  (z expansion),<sup>84</sup> "MuCap." <sup>86</sup>

The status of lattice-QCD calculations and examples of the phenomenological determinations of  $r_A^2$  are shown on the right-hand side of Fig. 5. The analysis with the z expansion<sup>84</sup> debunks the uncertainty estimates of determinations predicated on the dipole form. The model-independent results (red; between the horizontal lines) illustrate the best estimate of  $r_A^2$  without such strong assumptions. One should bear in mind that the "experimental" determinations all make assumptions: without new  $\nu d$  and  $\bar{\nu}p$  experiments, 85 it seems nearly impossible to improve the situation via experiment. On the other hand, lattice gauge theory can provide a first-principles results from QCD. However, currently, although lattice-QCD determinations of  $r_A^2$  are beginning to play a role, they are still quite sensitive to how the extrapolation is done, even with the z-expansion. Various determinations from different collaborations are quite different and likely there are still systematics that are not fully understood. However, they all lie within the range of the updated z-expansion  $r_A^2$  determination. 84,86 Another generation of calculations is needed before definitive results with uncertainties small enough to make an impact on cross-section calculations are achieved.

Nucleon isovector electromagnetic form factors: The nucleon isovector electromagnetic form factors are defined by

$$\langle N(p_f)|V_{\mu}^{+}(x)|N(p_i)\rangle = \bar{u}^N \left[\gamma_{\mu}F_1(q^2) + i\sigma_{\mu\nu}\frac{q^{\nu}}{2M_N}F_2(q^2)\right]u_N e^{iq\cdot x},$$
 (6)

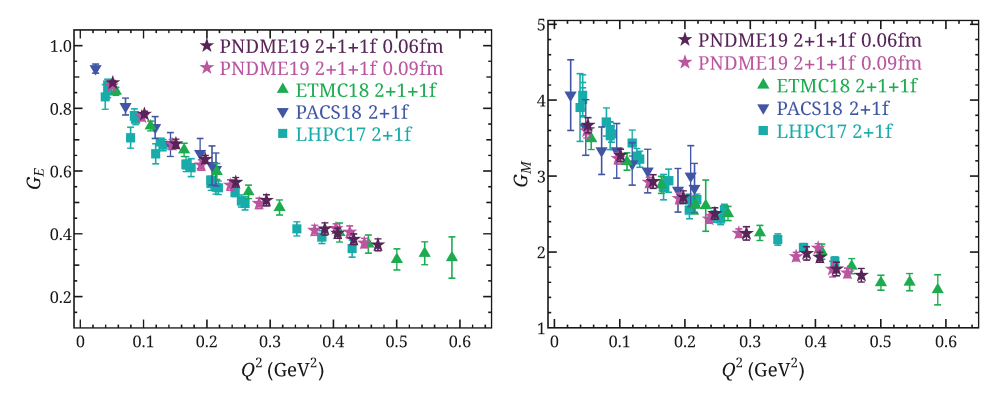


Fig. 6. Selected nucleon isovector electric (left) and magnetic (right) form factor results from near physical pion mass as functions of transferred momentum  $Q^2$ . The references corresponding to the above works are: 2f ETMC18<sup>94</sup> 2 + 1f LHPC14, 5 LHPC17, PACS18; 2 + 1 + 1f ETMC18, PNDME19<sup>96</sup> with 2 lattice spacings of 0.06 and 0.09 fm.

where the isovector current is  $V_{\mu}^{+}(x) = \bar{u}\gamma_{\mu}u - \bar{d}\gamma_{\mu}d$  and  $F_{1}$  and  $F_{2}$  are Dirac and Pauli form factors, respectively. The Sachs electric and magnetic form factors can be obtained from  $F_{1,2}$  as  $G_{E}(q^{2}) = F_{1}(q^{2}) + q^{2}F_{2}(q^{2})/(2M_{N})^{2}$  and  $G_{M}(q^{2}) = F_{1}(q^{2}) + F_{2}(q^{2})$ , which correspond to the Fourier transforms of nucleon charge and magnetization density distributions in the Breit frame. A precise knowledge of the charged-current versions of these quantities is essential to determine the neutrino–nucleon cross section. The intercepts and slopes of  $G_{E}^{\rm CC}$  and  $G_{M}^{\rm CC}$  are well determined from electromagnetic processes and isospin relations.

There are more lattice-QCD calculations of the electromagnetic form factors than the axial ones, inspired by the continuous experimental measurements. As a result, there are more calculations at physical pion mass for the electromagnetic form factors too. In Fig. 6, only selected results from near-physical pion masses are shown. PACS has the largest volume among these calculations and is able to probe the smallest  $Q^2$ . Overall, the lattice-QCD results among different collaborations are in good agreement within a couple standard deviations. The magnetic form factors have reasonable agreement with the experimental ones, but the electric form factors, depending on the analysis approach, have a small tension. With more precision experimental electric form factors on their way to resolve the proton radius puzzle, it would be nice to have lattice form factors at the percent level. To achieve this, one will need to include QED and isospin symmetry breaking in the lattice calculation, which will require significantly more computational resources.

### 3.3. Flavor-dependent nucleon structure

Nucleon structure in lattice QCD has long focused on isovector structure, where only the "connected" contributions (shown on the left-hand side of Fig. 7) are needed. To calculate flavor-dependent nucleon structure, we also need the "disconnected" contributions (shown on the right-hand side of Fig. 7), which are much

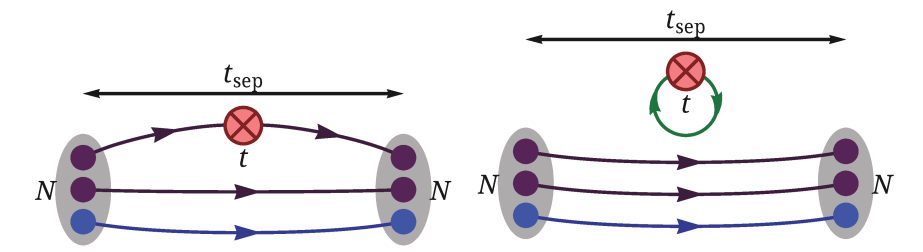


Fig. 7. The connected (left) and disconnected (right) three-point diagrams that contribute to the flavor-diagonal matrix elements of an operator (labeled by  $\otimes$  at time slice t). The gray blobs show the nucleon source and sink, separated by Euclidean time  $t_{\rm sep}$ . Sea-quark and gluon interactions, although present in the lattice configurations, are omitted from lattice propagator diagrams such as this.

more numerically challenging, requiring algorithm development and high statistics to get any signal out of the calculations. There have been significant advances in numerical techniques and improvements to computational hardware that make this possible, with some calculations even taking place close to the physical quark masses. A couple examples are highlighted in this subsection, focusing on results that include a proper continuum limit and those with interesting applications or implications.

Quark Contribution to the Proton Spin: After decades of experimental effort one remaining mystery of QCD is: How are sea quarks and gluons, and their spins, distributed in space and momentum inside the nucleon? The attempts to answer this question have resulted in numerous experimental efforts: In the US alone, physics targets are being pursued by multiple DOE laboratories, BNL and JLab, as well as the future EIC.

The proton spin is dominated by quark intrinsic spin; each quark flavor q = u, d, s contributes  $\Delta q \equiv \Delta \Sigma_q \equiv \langle 1 \rangle_{\Delta q^+} \equiv g_A^q$  to the nucleon spin. Experimentally, one needs to measure the helicity distributions  $(\Delta q(x) + \Delta \bar{q}(x))$  as a function of Bjorken-x and take the first Mellin moment of the PDF by integrating over x:<sup>36</sup>

$$\Delta q = \int_0^1 dx (\Delta q(x) + \Delta \bar{q}(x)). \tag{7}$$

The quark spins are also important to quantify the strength of the spin-dependent interaction of dark matter with nucleons. <sup>97,98</sup> Among the quark spins,  $\Delta s$  is the least well known and current analyses <sup>36</sup> often rely on assumptions such as SU(3) symmetry and  $\Delta s = \Delta \bar{s}$ . On the lattice,  $\Delta q$  can be calculated via the matrix element of the flavor-diagonal axial current,  $\bar{q}\gamma_{\mu}\gamma_{5}q$ :

$$\Delta q \bar{u}_N \gamma_\mu \gamma_5 u_N = \langle N | Z_A \bar{q} \gamma_\mu \gamma_5 q | N \rangle , \qquad (8)$$

where  $Z_A$  is the renormalization constant and  $u_N$  is the nucleon spinor. The total quark spin contribution to the proton is then  $\frac{1}{2}\Delta\Sigma \equiv \sum_{q=u,d,s} \frac{1}{2}\Delta q$ .

To provide reliable input, lattice-QCD calculations must take into account all systematics mentioned in Sec. 2 as well as overcome the numerical challenges of statistical noise in the disconnected nucleon three-point contributions. Reference 99 used 4 lattice spacings  $\{0.15, 0.12, 0.09, 0.06\}$  fm including ensemble at physical pion mass to study the quark spin contribution to the proton spin. High-statistics calculations are performed for both the connected and disconnected contributions to the nucleon three-point functions using the following strategy: the quark-disconnected diagrams are estimated using a stochastic method accelerated with a combination of the truncated-solver method (TSM), 100,101 the hopping-parameter expansion (HPE)<sup>102,103</sup> and the all-mode-averaging (AMA) technique. <sup>104</sup> This method of calculating quark-disconnected contributions to nucleon charges has proven to be useful in extracting the up, down and strange contributions to nucleon tensor charges, and set an upper bound for BSM scenarios that are dominated by quark EDM. 4,105 A more detailed description of the numerical techniques used can be found in Refs. 1 and 4. An important finding of this work is that the lattice discretization errors and the chiral corrections are large; consequently, evaluating the renormalized charges at the physical pion mass and extrapolating to the continuum limit are essential. The "disconnected" contributions due to light/strange quarks,  $g_A^{l,\mathrm{disc}}$  and  $g_A^{s,\,\mathrm{disc}}$  are calculated with high statistics with  $O(10^3)$  configurations and  $O(10^4)$  random sources in Ref. 99. After proper renormalization, these disconnected contributions to the quark charges are simultaneously extrapolated to the physical limit using the ansatz,

$$g_A^{q, \text{disc}}(a, M_\pi, L) = c_0 + c_a a + c_M M_\pi^2$$
. (9)

 $c_0$  parameter gives the disconnected contributions in the chiral limit, -0.129(15) and -0.058(9) for light and strange, respectively. For both charges, as expected, a nonzero dependence on quark mass,  $c_M$ , is found 0.53(15) and 0.22(10) GeV<sup>-2</sup>. However, although  $c_a$  is usually set to zero in many lattice-structure calculations, the coefficient dependent on lattice spacing,  $c_a$ , is not small compared with the magnitude of the disconnected part of the charges, 0.207(88) and 0.084(65) fm<sup>-1</sup>. This suggests that using ensembles at multiple lattice spacings is very important to obtain the correct quark spin contribution. Without taking the continuum extrapolation, one can easily miss a factor of 2 or more in the disconnected charges, resulting in a wrong picture of the proton spin decomposition.

The extrapolation fit including some next-order corrections,  $a^2$  for the discretization error and  $M_{\pi}^2 \log M_{\pi}^2$  for the chiral log term, are also included one at a time. In each case, the errors in the fitted coefficients and extrapolated results grow as expected. For example, in the best case of adding the  $a^2$  term will change  $g_A^{l,\text{disc}} = -0.147(43)$  from -0.118(14), and the lattice-spacing coefficients  $c_a = 0.67(71)$  and  $c_{a^2} = -2.1(3.2)$  when a is replaced by  $a^2$  in the extrapolation formula. PNDME's final results are derived from fits using Eq. (9) but account for the uncertainty in the fit model by assigning an additional systematic error of 0.03.

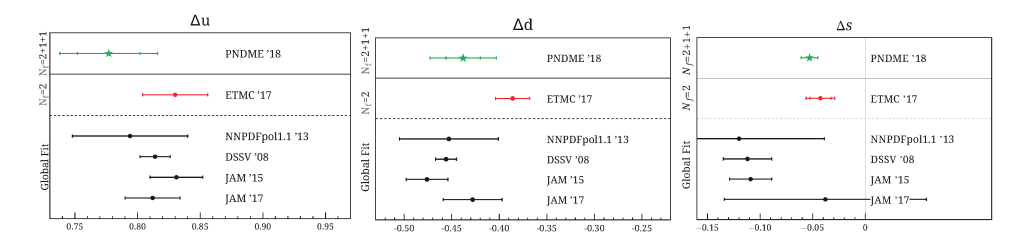


Fig. 8. Summary of results on  $\Delta u$  (left),  $\Delta d$  (middle) and  $\Delta s$  (right) with lattice chiral-continuum extrapolated PNDME'18 results<sup>99</sup> compared with ETMC values from a single lattice spacing, <sup>106,107</sup> and with moments from global fits to polarized PDF (NNPDFpol1.1'13, <sup>109</sup> DSSV'08, <sup>110,111</sup> Jam'15, <sup>112</sup> and JAM'17<sup>113</sup>). All PDF results are taken from Ref. 36 and are in the  $\overline{\rm MS}$  scheme at 2 GeV. These plots are taken from the original works in Ref. 99.

Figure 8 shows a summary of the lattice results at physical-mass ensembles and the moments extracted from global fits to the polarized PDFs reviewed in Ref. 36. Within errors, the lattice results are compatible with the moments extracted from global PDF fits which are renormalized in the  $\overline{\rm MS}$  scheme at 2 GeV. The ETMC lattice results derive from a single physical-mass 2-flavor ensemble at  $a=0.093~{\rm fm},^{106,107}$  while the PNDME'18 work is done using eleven ensembles with proper continuum extrapolation. There are some small differences between the results from these 2 groups, which can be accounted for by the a dependence highlighted in the disconnected-contribution data observed in Fig. 3 of Ref. 99. Reference 99 shows noticeable differences with and without continuum extrapolation, especially in discretization errors.

High-statistics results from Ref. 99 on each ensemble for all three quantities allow one to quantify systematic uncertainties and perform a simultaneous chiral-continuum extrapolation in the lattice spacing and the light-quark mass:  $\Delta u \equiv \langle 1 \rangle_{\Delta u^+} = 0.777(25)(30), \ \Delta d \equiv \langle 1 \rangle_{\Delta d^+} = -0.438(18)(30), \ \text{and} \ \Delta s \equiv \langle 1 \rangle_{\Delta s^+} = -0.053(8) \ \text{with statistical (first error) and systematic uncertainty associated with the chiral-continuum extrapolation (second error). Adding up the total quark contribution to proton spin of <math>\sum_{q=u,d,s}(\frac{1}{2}\Delta q) = 0.143(31)(36)$ . These results are obtained without model assumptions and are in good agreement with the recent COMPASS analysis  $0.13 < \frac{1}{2}\Delta \Sigma < 0.18$ . Scaling the value of  $g_A^s$  by  $1/m_q$  predicts that the neglected charm contribution could be  $g_A^c \approx -0.005$ .

Implications for the Neutron Electric Dipole Moment (EDM): Searches for a neutron permanent EDM  $d_n$  have high sensitivity to CP-violating interactions beyond the Standard Model (BSM). At the hadronic scale around 1 GeV, after integrating out all heavy degrees of freedom, the dominant effect of new CP-violating couplings in BSM theories is encoded in local operators of dimension five and six. Leading, among them, are the elementary fermion EDMs: $^{114,115}$ 

$$\delta \mathcal{L}_{\text{CPV}} \supset -\frac{ie}{2} \sum_{f=u,d,s,e} d_f \bar{f} \, \sigma_{\mu\nu} \gamma_5 F^{\mu\nu} f \,.$$
 (10)

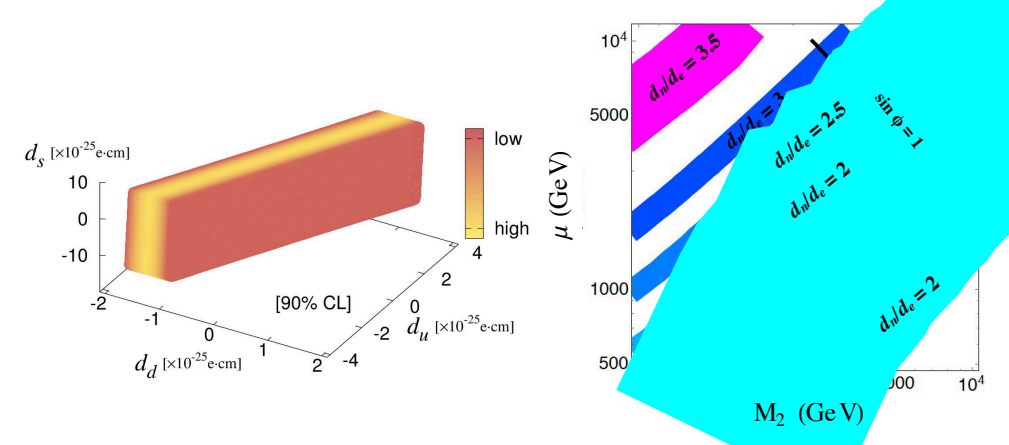


Fig. 9. (Left) Constraints on the BSM couplings of the CP-violating quark EDM operator using the current experimental bound on the nEDM  $(2.9 \times 10^{-26} e \cdot \text{cm}^{119})$ . The strongest constraint is a strip in  $d_u$  and  $d_d$ , i.e. representing the thickness of the slab, with high (low) corresponding to a p-value of 1 (0.1). (Right) Regions in  $M_2$ - $\mu$  plane corresponding to various values of  $d_n/d_e$  in split SUSY, obtained by varying  $g_T^{u,d,s}$  within our estimated uncertainties. For  $\mu$ ,  $M_2 > 500$  GeV, maximizing the ratio  $d_n/d_e$  along this line gives the upper bound  $d_n < 4.1 \times 10^{-29} e \cdot \text{cm}$  at  $d_n/d_e = 3.71$ . Figures taken from Ref. 118.

The contribution of the quark EDM  $d_q$  to  $d_n$  is  $^{116,117}$ 

$$d_n = g_T^u d_u + g_T^d d_d + g_T^s d_s \,.$$
(11)

However, tensor-charge information has been hard to obtain precisely from experiments to date; therefore, combining improved knowledge of  $g_T^q$  from lattice QCD with experimental bounds on  $d_n$  can provide stringent constraints on new CP-violation encoded in  $d_q$ .

Reference 105 presents the lattice-QCD results on the neutron up/down/strange tensor charges including, for the first time, a simultaneous extrapolation in the lattice spacing, volume, and light-quark masses to the physical point in the continuum limit. The calculation was updated with up to 11 lattice ensembles in 2018, including 4 lattice spacings and improved statistics. Using the lattice tensor charges at the physical limit and the experimental bound on the nEDM ( $d_n \leq 2.9 \times 10^{-26}~e\cdot {\rm cm}^{119}$ ), the Eq. (11) provides constraints on the CP violating quark EDMs,  $d_q^{\gamma}$ , arising in BSM theories, assuming that the quark EDM is the only CP-violating BSM operator. The bounds on  $d_q^{\gamma}$  are shown in the left panel of Fig. 9. Of particular importance is the reduction in the error in  $g_T^s = 0.0027(16)$  from Ref. 118 compared to the previous result,  $d_q^{\gamma} = 0.008(9)$ , which leads to bounds on  $d_s^{\gamma}$  even though  $d_s^{\gamma}$  remains noisy. Conversely, the overall error in  $d_n$  is reduced even if  $d_s^{\gamma}$  is enhanced versus  $d_u^{\gamma}$  by  $m_s/m_u \approx 40$ , as occurs in models in which the chirality flip is provided by the Standard Model Yukawa couplings.

In general, BSM theories generate a variety of CP-violating operators that all contribute to  $d_n$  with relations analogous to Eq. (11). As discussed in Ref. 105, in the "split SUSY" model, <sup>120–122</sup> the fermion EDM operators provide the dominant

BSM source of CP violation. The right-hand side of Fig. 9 shows the contour plots for  $d_n/d_e$  in the gaugino-mass  $(M_2)$  and higgsino-mass  $(\mu)$  parameter plane over the range 500 GeV to 10 TeV. For this analysis, we have followed Ref. 123 and set  $\tan \beta = 1$ .

Thanks to the greatly reduced uncertainty in the tensor charges (factor of  $\approx 6$  for  $g_T^s$  and  $\approx 2$  for  $g_T^{u,d}$ ), the ratio  $d_n/d_e$  is much more precisely known in terms of SUSY mass parameters. This allows for stringent tests of the split SUSY scenario with gaugino mass unification.  $^{120-122}$  In particular, our results and the experimental bound  $d_e < 1.1 \times 10^{-29} e \cdot \text{cm}$ ,  $^{124,125}$  imply the split-SUSY upper bound  $d_n < 4.1 \times 10^{-29} e \cdot \text{cm}$ . This limit is falsifiable by next-generation nEDM experiments. Constraints on split SUSY from LHC searches predicated on gluino decays rule out the region below about a TeV in the  $\{\mu, M_2\}$  plane,  $^{126}$  whereas, assuming a maximal CP-violating phase ( $\sin \phi = 1$ ), EDMs currently probe scales considerably higher than LHC's energy scale reach.

### 4. Bjorken-x-Dependent Hadron Structure

The formulation of lattice QCD in Euclidean space has severely restricted lattice calculations of partonic structure for decades. However, much exciting progress has been made in recent years. "Large-Momentum Effective Theory" (LaMET), 18,127 was proposed to overcome the limitations of lattice QCD by computing spatially extended equal-time matrix elements with large momentum in the external states, as shown in Eq. (1). The quasi-PDF is obtained by Fourier transforming these nonperturbatively renormalized matrix elements to momentum space. To relate this lattice quasi-PDF to the desired Minkowski lightcone PDF, matching conditions are implemented within LaMET. Power corrections that break the matching procedure from higher-twist effects are suppressed at large nucleon momentum. A variety of other approaches were investigated soon after the quasi-PDF calculations: the "pseudo-PDF" approach considers the ratio of equal-time matrix elements of the Wilson line between quarks with the rest-frame density matrix element and is parametrized in terms of the "Ioffe time," 128,129 focusing on the Ioffe-time distribution; <sup>130,131</sup> the "good lattice cross sections" approach <sup>132,133</sup> uses singlehadron matrix elements of a time-ordered, renormalized nonlocal operator  $\mathcal{O}_n(z)$ :  $\sigma_n(\nu, z^2, p^2) = \langle p|T\{\mathcal{O}_n(z)\}|p\rangle$  with four-vector momentum, which can cover a wider variety of matrix elements; the "hadronic-tensor" approach 13,14,17,134,135 accesses partonic distributions through a discrete Laplace transform of the Euclidean hadronic tensor; the "fictitious heavy-quark field" approach extends the corresponding hadronic tensor involving heavy-light currents and resulting lattice correlation functions are matched on to the relevant operator product expansion (OPE) to extract the moments of regular parton distributions; <sup>136</sup> other approaches based on transforms of the hadronic tensor are being pursued in Refs. 137. These calculations only started a few years ago; even though there have been interesting results reported every year, not all the required lattice-QCD systematics have been

taken into account. Results are mostly limited to a few lattice ensembles for now; one should keep in mind that the actual systematics if included could be much larger than currently estimated. Among various new methods, LaMET approach, which calculates boosted hadron matrix elements at multiple spatial displacements, shows promising PDFs at physical pion mass, calculated by both LP<sup>3</sup> and ETMC collaborations. Due to the limited space, in this review, only quasi-PDF results are shown.

In the LaMET (or "quasi-PDF") approach, time-independent spatially displaced matrix element that can be connected to PDFs are computed, and the operator choice is not unique at finite hadron momentum  $P_z$ . A convenient choice for leading-twist PDFs is to take the hadron momentum and quark—antiquark separation to be along the z direction

$$h_{\Gamma}(z, p_z) = \frac{1}{4p_z} \sum_{s=1}^{2} \langle p, s | \bar{\psi}(z) \Gamma e^{ig \int_0^z A_z(z') dz'} \psi(0) | p, s \rangle, \qquad (12)$$

where  $p_z$  is the hadron momentum boosted in the z direction, s its spin, and z is the separation of the quark and antiquark fields  $\bar{\psi}$  and  $\psi$ . There are multiple choices of operator in this framework that will recover the same lightcone PDFs when the large-momentum limit is taken. For example,  $\Gamma$  can be  $\gamma_z$  or  $\gamma_t$ ;  $^{130,131,138,139}$  both will give the unpolarized PDFs in the infinite-momentum frame. Since the first lattice Bjorken-x dependent PDF calculation,  $^{19}$  there have been many follow-up works, leading to rapid developments in the direct calculation of the Bjorken-x dependence of hadron structure using lattice QCD; the technique shows promising results. On the lattice side, more lattice-QCD calculations of the nucleon isovector quark distributions  $^{19-21,26,139-142}$  have been reported since, including the unpolarized, polarized and transversity cases and variations of the quasi-PDF methods. Results at physical pion mass were first reported in  $2017^{143}$  and many additional studies followed.  $^{2,22,23,144-146}$  Recently, there have also been a number of works on quasi-PDF renormalization.  $^{141,142,147-156}$ 

Nucleon Parton Distribution Functions at Physical Pion Mass: In this review, the work of LP<sup>3</sup> collaboration is highlighted, since they pioneered many quantities and include systematic errors in the PDF results. We first consider their lattice calculations of the bare isovector quark unpolarized, helicity, and transversity quasi-PDFs using clover valence fermions<sup>4,46,92,105</sup> on an ensemble of gauge configurations with lattice spacing a = 0.09 fm, box size  $L \approx 5.8$  fm, and with pion mass  $M_{\pi} \approx 135$  MeV and  $N_f = 2 + 1 + 1$  (degenerate up/down, strange and charm) flavors of highly improved staggered dynamical quarks (HISQ)<sup>157</sup> generated by MILC Collaboration.<sup>80</sup> Gaussian momentum smearing<sup>158</sup> is used for the quark field to increase the overlap of the lattice sources with the ground state of the large-boost nucleon. For the nucleon matrix elements of  $\hat{O}(z, a)$  at a given boost momentum,  $\tilde{h}(z, P_z, a)$ , the ground-state matrix elements are extracted from each

three-point correlator,  $C_{\Gamma}^{(3\text{pt})}(P_z, t, t_{\text{sep}})$  by fitting the following form:

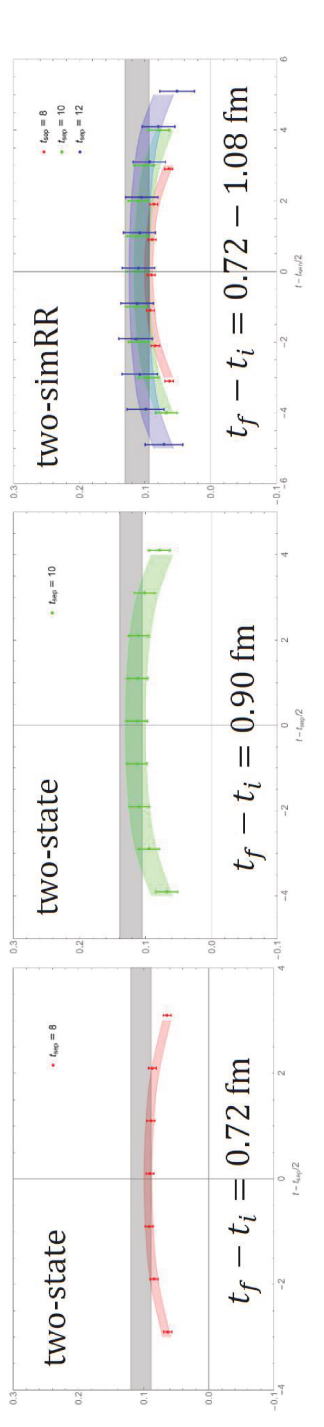
$$\begin{split} C_{\Gamma}^{\mathrm{3pt}}(P_z,t,t_{\mathrm{sep}}) &= |\mathcal{A}_0|^2 \langle 0|\mathcal{O}_{\Gamma}|0\rangle e^{-E_0 t_{\mathrm{sep}}} + |\mathcal{A}_1|^2 \langle 1|\mathcal{O}_{\Gamma}|1\rangle e^{-E_1 t_{\mathrm{sep}}} \\ &+ |\mathcal{A}_1||\mathcal{A}_0| \langle 1|\mathcal{O}_{\Gamma}|0\rangle e^{-E_1 (t_{\mathrm{sep}} - t)} e^{-E_0 t} \\ &+ |\mathcal{A}_0||\mathcal{A}_1| \langle 0|\mathcal{O}_{\Gamma}|1\rangle e^{-E_0 (t_{\mathrm{sep}} - t)} e^{-E_1 t} + \cdots, \end{split}$$

where the operator is inserted at time t, and the nucleon state is annihilated at the sink time  $t_{\rm sep}$ , which is also the source-sink separation (after shifting source time to zero). The state  $|0\rangle$  represents the ground state and  $|n\rangle$  with n>0 the excited states. In our two-state fits, the amplitudes  $\mathcal{A}_i$  and the energies  $E_i$  are functions of  $P_z$  and can be obtained from the corresponding two-point correlators. Figure 10 shows one of the many studies of excited-state contamination, performing fits with and without the  $\langle 1|\mathcal{O}_{\Gamma}|1\rangle$  contribution (labeled as "two-simRR" and "two-sim," respectively) and using data from different source-sink separations  $t_{\rm sep}$ .<sup>2,23,144</sup>

The nonperturbative renormalization (NPR) factor  $\tilde{Z}(z,p_z^R,\mu_R,a)$  is calculated from the amputated Green function of  $\hat{O}(z,a)$  with a similar procedure, <sup>144,159</sup> where  $p_z^R$  and  $\mu_R$  are the Euclidean quark momentum in the z-direction and the off-shell quark momentum, respectively. The bare matrix element of  $\hat{O}(z,a)$ ,  $\tilde{h}(z,P_z,a)$ , has ultraviolet (UV) power and logarithmic divergences as  $a\to 0$  and must be nonperturbatively renormalized to have a well defined continuum limit. Next, the renormalized matrix elements  $h_R(z,P_z,p_z^R,\mu_R)$  are Fourier transformed into x-space to obtain the quasi-distribution  $\tilde{q}(x,P_z,p_z^R,\mu_R)$ :

$$\tilde{f}(x, 1/a, p_z) = \int \frac{dz}{2\pi} e^{-ixzp_z} p_z h_{\Gamma}(z, p_z). \tag{13}$$

As originally pointed out in 2017 and demonstrated using CT14 NNLO $^{160}$  at 2 GeV, a naive Fourier transform from momentum-space x to coordinate space z and then back suffers an inverse problem<sup>143</sup> (see the left-hand side of Fig. 11). The oscillation is less noticeable if calculation stays in the small- $P_z$  region, as shown in the pink band in the figure. This means that since the lattice calculation has finite displacement z in the nonlocal operator and cannot actually use infinitely boosted momentum, a straightforward Fourier transform produces truncation effects, resulting in unphysical oscillatory behavior, as observed in earlier works. 141,142 The antiquark and small-x regions suffer the maximum deformation. Two ideas ("filter" and "derivative" methods)<sup>143</sup> were originally proposed to remove this biggest systematic uncertainty in the LaMET approach to studying x-dependent hadron structure: Fourier-transformation truncation. When not assuming a parametrization form, this determines the shape of the PDF. The first lattice PDF at physical pion mass was used to demonstrate how the proposed methods improve real-world lattice calculations. A third method was proposed in late 2017, modifying the Fourier transformation in LaMET using a single-parameter Gaussian weight. <sup>161</sup> In 2019, another three methods were proposed. 162 Following the recent work, 2,23,144 the simple but



This figure shows the consistency between two-state fits truncated at different terms and different  $t_{\rm sep}$  data for the case of transversity matrix elements at z = 3,  $P_z = 2.6$  GeV at physical pion mass. Fig. 10.

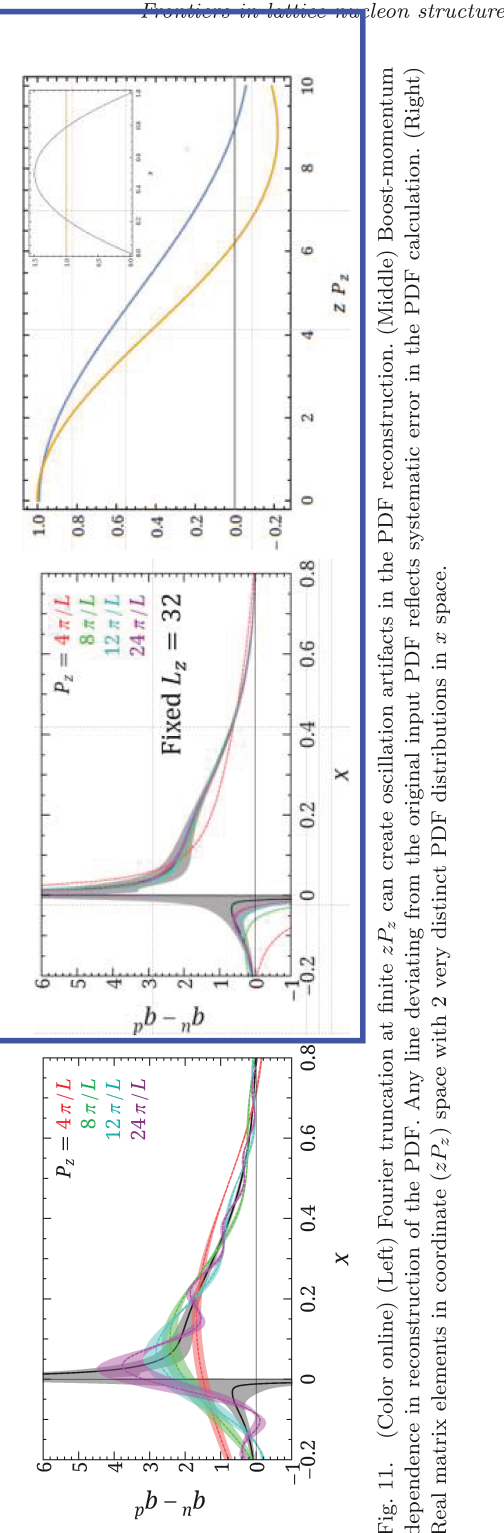


Fig. 11. (Color online) (Left) Fourier truncation at finite  $zP_z$  can create oscillation artifacts in the PDF reconstruction. (Middle) Boost-momentum dependence in reconstruction of the PDF. Any line deviating from the original input PDF reflects systematic error in the PDF calculation. (Right) Real matrix elements in coordinate  $(zP_z)$  space with 2 very distinct PDF distributions in x space.

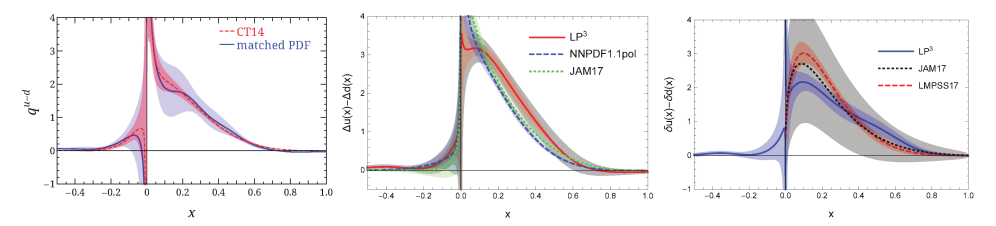


Fig. 12. (Color online) LP<sup>3</sup>'s isovector unpolarized (left),<sup>23</sup> helicity (middle)<sup>2</sup> and transversity (right)<sup>144</sup> PDFs renormalized at 3 GeV in comparison with global-fit PDFs.

effective "derivative" method is adopted here:

$$\tilde{Q}(x, P_z, p_z^R, \mu_R) = i \int_{-z_{\text{max}}}^{+z_{\text{max}}} dz \, e^{ixP_z z} \tilde{h}'_R(z, P_z, p_z^R, \mu_R) / x \,,$$
 (14)

where  $\tilde{Q}$  is the quasi-PDF  $(q(x), \Delta q(x))$  and  $\delta q(x)$  respectively), and  $\tilde{h}'_R$  is the derivative of the renormalized matrix elements for the corresponding operator. One immediately notices that when  $P_z$  is small, the sea-quark asymmetry would come out of lattice calculation with the wrong sign, which is exactly what was seen in the low- $P_z$  PDF calculations,  $^{22,143}$  in addition to missing the small-x region. There are a number of proposals to avoid the Fourier transformation by working in position space; this would work in an ideal world when there is sufficiently precise data throughout the large- $zP_z$  region. However, in reality, the lattice data taken in the small- $zP_z$  region is not precise enough to even discern whether the parton distribution is flat across all x; one loses sensitivity to two very distinct distributions in x-space, which now become very similar in  $zP_z$  space. Furthermore, one still needs large  $zP_z$  to reliably obtain the distribution in the small-x region. It would be great to have a systematic way to demonstrate the lattice data inputs in  $zP_z$  space.

Once the quasi-PDFs is obtained, they can be related to the true lightcone PDFs using the matching condition

$$\tilde{q}(x, \Lambda, p_z) = \int_{-1}^{1} \frac{dy}{|y|} Z\left(\frac{x}{y}, \frac{\mu}{p_z}, \frac{\Lambda}{p_z}\right)_{\mu^2 = Q^2} q(y, Q^2) + O\left(\frac{\Lambda_{\text{QCD}}^2}{p_z^2}, \frac{M^2}{p_z^2}\right), \quad (15)$$

where  $\mu$  is the renormalization scale, Z is a matching kernel and M is the hadron mass. Here, the  $O(M^2/p_z^2)$  terms are target-mass corrections and the  $O(\Lambda_{\rm QCD}^2/p_z^2)$  terms are higher-twist effects, both of which are suppressed at large hadron momentum. Early exploratory works have shown great promise in obtaining quantitative results for the unpolarized, helicity and transversity quark and antiquark distributions. The first LaMET PDFs at physical pion mass were done using small momentum ( $P_z^{\rm max} \approx 1.3~{\rm GeV}$ ); as described earlier, one expects the wrong sign of sea-flavor asymmetry to be seen in the Fourier transformation. Figure 12 shows the newer PDF results on ensembles at physical pion mass with momenta above 2 GeV, and then renormalized at 3 GeV. The error band displayed here includes the systematic error coming from variations in the renormalization scale,  $zP_z$  in the Fourier transformation, estimation of lattice spacing and finite-volume

effects from other nucleon matrix studies and the matching formula approximation. As expected from the Fourier-transformation study, the sea-flavor asymmetry is recovered with increased momentum. In the positive isovector quark region, the lattice results agree nicely with CT14,  $^{160}$  which is consistent with NNPDF3.1  $^{163}$  and CJ15,  $^{164}$  up to the small-x region, where even larger  $zP_z$  data is required for lattice calculation to have control over these regions. The middle plot of Fig. 12 shows LP³'s isovector quark helicity PDF² matched in  $\overline{\rm MS}$ -scheme at scale  $\mu=3$  GeV, extracted from LaMET at the largest proton momentum (3 GeV), compared with fits by NNPDFpol1.1  $^{109}$  and JAM.  $^{113}$  The red band denotes statistical error, while the gray band also includes systematics. The right-hand side of Fig. 12 shows LP³'s proton isovector transversity PDF¹44 at renormalization scale  $\mu=\sqrt{2}$  GeV ( $\overline{\rm MS}$  scheme), extracted from lattice QCD and LaMET at  $P_z=3$  GeV, compared with global fits by JAM17 and LMPSS17.  $^{10}$  The blue error band includes statistical errors (which fold in the excited-state uncertainty) and systematics mentioned in the unpolarized PDF cases.

Gluon PDFs: The unpolarized gluon PDF is defined by the Fourier transform of the lightcone correlation in the hadron,

$$g(x,\mu^2) = \int \frac{\mathrm{d}\xi^-}{\pi x} e^{-ix\xi^- P^+} \langle P|F_\mu^+(\xi^-)U(\xi^-,0)F^{\mu+}(0)|P\rangle , \qquad (16)$$

where  $\xi^{\pm} = \frac{1}{2}(\xi^0 \pm \xi^3)$  is the spacetime coordinate along the lightcone direction, the hadron momentum  $P_{\mu} = (P_0, 0, 0, P_z)$ ,  $|P\rangle$  is the hadron state with momentum P with the normalization  $\langle P|P\rangle = 1$ ,  $\mu$  is the renormalization scale, and  $F_{\mu\nu} = T^a G^a_{\mu\nu} = T^a \left(\partial_{\mu}A^a_{\nu} - \partial_{\nu}A^a_{\mu} - gf^{abc}A^b_{\mu}A^c_{\nu}\right)$  is the gluon field tensor;  $U(\xi^-, 0) = \mathcal{P} \exp\left(-ig\int_0^{\xi^-} \mathrm{d}\eta^- A^+(\eta^-)\right)$  is the lightcone Wilson link from  $\xi^+$  to 0 with  $A^+$  as the gluon potential in the adjoint representation. However, these time-separated and nonlocal operators cannot be directly calculated using lattice QCD. LQCD has only been used to calculate the first moment of the gluon PDF<sup>106,165–168</sup> and calculations of moments beyond the first are still absent.

Given the recent success in the quark sector of the LaMET calculation as described in above, it is time to explore how this would work for the gluon. <sup>169</sup> Focusing on the unpolarized gluon PDF, the LaMET quasi-PDF can be obtained through

$$\tilde{g}(x, P_z^2)(\mu) = \int \frac{\mathrm{d}z}{\pi x} e^{-ixzP_z} Z(\mu, z) \tilde{H}_0(z, P_z),$$
(17)

where  $\tilde{H}_0(z, P_z) = \langle P | \mathcal{O}_0 | P \rangle$  and

$$\mathcal{O}_0 \equiv \frac{P_0(\mathcal{O}(F_\mu^t, F^{\mu t}; z) - \frac{1}{4}g^{tt}\mathcal{O}(F_\nu^\mu, F_\mu^\nu; z))}{\frac{3}{4}P_0^2 + \frac{1}{4}P_z^2}, \tag{18}$$

with the correlation operator  $\mathcal{O}(O_1, O_2; z)$  defined by  $O_1(z)U(z, 0)O_2(0)$ . The renormalization constant in the so-called "ratio" scheme  $Z(\mu, z) = Z_{gg}^{\overline{\text{MS}}}(\mu)\tilde{H}_0(0, 0)/\tilde{H}_0(z, 0)$  cancels all the UV divergence in  $\tilde{H}(z, P_z)$ , including the linear term<sup>149</sup>

due to the Wilson line under the lattice regularization, where  $Z_{gg}^{\overline{\text{MS}}}(\mu)$  is the  $\overline{\text{MS}}$  renormalization constant of  $\langle x \rangle_q$  at the scale  $\mu$ .

The choice for the quasi-PDF operator is not unique. Any operator that approaches the lightcone one in the large-momentum limit is a possible candidate, like the choice inspired by operators used in the moment definition but with a long displacement along the boost momentum direction:

$$\mathcal{O}_{1}(z) \equiv \frac{1}{P_{z}} \mathcal{O}(F_{\mu}^{t}, F^{z\mu}; z) , 
\mathcal{O}_{2}(z) \equiv \frac{P_{0}(\mathcal{O}(F_{\mu}^{z}, F^{\mu z}; z) - \frac{1}{4}g^{zz}\mathcal{O}(F_{\nu}^{\mu}, F_{\mu}^{\nu}; z))}{\frac{1}{4}P_{0}^{2} + \frac{3}{4}P_{z}^{2}} ,$$
(19)

as well as

$$\mathcal{O}_3(z) \equiv \frac{1}{P_0} \mathcal{O}(F_\mu^z, F^{z\mu}; z) \,,$$
 (20)

proposed by Ref. 18. As discussed in Ref. 169, the quasi-PDF using  $\mathcal{O}_{1,2,3}$  has larger higher-twist corrections and statistical uncertainty compared to that using  $\mathcal{O}_0$ .

In the first exploratory study,<sup>169</sup> ensembles with unphysically heavy quark masses were used. Since gluon quantities are much noisier even than quark disconnected loops, cheap calculations with very high statistics are necessary to have any hope of seeing signal. The calculations were done using overlap fermions on gauge ensembles with 2+1 flavors of domain-wall fermion and spacetime volume  $24^3 \times 64$ , a = 0.1105(3) fm, and  $M_{\pi}^{\rm sea} = 330$  MeV. The gluon operators were calculated for using all volumes and high statistics: 207,872 measurements were taken of the two-point functions with valence quarks at the light sea and strange masses (corresponding to pion masses 340 and 678 MeV, respectively). On the lattice, the field tensor  $F_{\mu\nu}$  needed for the quasi-PDF operator  $\mathcal{O}_{0,1,2,3}$  is

$$F_{\mu\nu} = \frac{i}{8a^2g} \left( \mathcal{P}_{[\mu,\nu]} + \mathcal{P}_{[\nu,-\mu]} + \mathcal{P}_{[-\mu,-\nu]} + \mathcal{P}_{[-\nu,\mu]} \right), \tag{21}$$

where the plaquette  $\mathcal{P}_{\mu,\nu} = U_{\mu}(x)U_{\nu}(x+a\hat{\mu})U_{\mu}^{\dagger}(x+a\hat{\nu})U_{\nu}^{\dagger}(x)$  and  $\mathcal{P}_{[\mu,\nu]} = \mathcal{P}_{\mu,\nu} - \mathcal{P}_{\nu,\mu}$ . The  $F_{\mu\nu}$  are very noisy, so to further improve the signal of  $H_g$ , up to 5 steps of hypercubic (HYP) smearing are applied to the gluon operators.

The  $\overline{\rm MS}$  renormalized gluon quasi-PDF matrix element  $\tilde{H}^{\overline{\rm MS}}(z,P_z,\mu)$  can be factorized into the perturbatively calculable matching kernel C and the lightcone PDF g(x) through a factorization theorem<sup>147,170</sup> up to higher-twist corrections at  $O\left(z^2\Lambda_{\rm QCD}^2\right)$  and mixing with the quark PDF at  $O(\alpha_s(\mu))$ ,

$$\widetilde{H}^{\overline{\mathrm{MS}}}(z, P_z, \mu) = \int \mathrm{d}\xi \, C(\xi, z^2, \mu^2) H(\xi z P_z, \mu) + O(z^2 \Lambda_{\mathrm{QCD}}^2) + O(\alpha_s(\mu)), \quad (22)$$

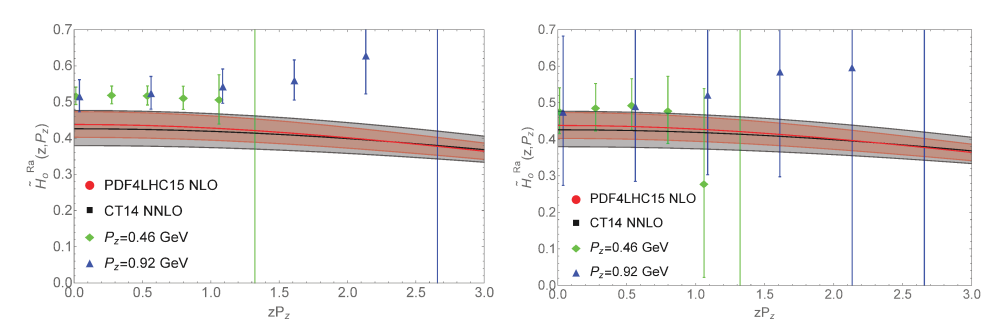


Fig. 13. The final results of  $\tilde{H}_0^{Ra}(z,P_z)$  at 678 MeV (top) and 340 MeV (bottom) pion mass as functions of  $zP_z$ , compared with the FT of the gluon PDF from the global fits PDF4LHC15<sup>172</sup> and CT14.<sup>160</sup> They are consistent with each other within the uncertainty.

with  $H(\omega, \mu) = \int_0^1 e^{i\omega x} x g(x) dx$ . The renormalized gluon quasi-PDF matrix element  $\tilde{H}_0^{Ra}(z, P_z, \mu) \equiv Z(\mu, z) \tilde{H}_0(z, P_z)$  in the ratio scheme can also be factorized by

$$\tilde{H}_{0}^{Ra}(z, P_{z}, \mu) = \int d\xi \frac{C(\xi, z^{2}, \mu^{2})}{\int d\beta C(\beta, z^{2}, \mu^{2})} H(\xi z P_{z}, \mu) 
+ O(z^{2} \Lambda_{QCD}^{2}) + O(\alpha_{s}(\mu)),$$
(23)

using the fact that  $H(0,\mu) = \langle x \rangle_g^{\overline{\text{MS}}}(\mu)$ . As shown in previous calculations, <sup>148,171</sup> the mixing contribution from the quark PDF can be important, and future studies should investigate these effects.

Finally, the coordinate-space gluon quasi-PDF matrix element ratios are plotted in Fig. 13, compared with the corresponding Fourier transform of the gluon PDF based on the global fits from NLO PDF4LHC15<sup>172</sup> and CT14.<sup>160</sup> Up to perturbative matching and power correction at  $O(1/P_z^2)$ , they should be the same, and our simulation results are within the statistical uncertainty at large z. The results at the lighter pion mass (at the unitary point) of 340 MeV are also shown in Fig. 13, which is consistent with those from the strange point but with larger uncertainties. The pion gluon quasi-PDFs were also studied for the first time in Ref. 169 and similar features as the nucleon counterpart is observed as well. There have been recent developments in improving the operators for the gluon-PDF lattice calculations,  $^{173-175}$  which will allow us to take the continuum limit for the gluon PDFs in future lattice calculations.

#### 5. Conclusions and Outlook

It is an exciting era for lattice nucleon-structure calculations. On one hand, the traditional charge and moment calculations have been done at physical pion mass in recent years, and more collaborations are looking into studying systematics using multiple lattice spacings and volumes. The first rating of nucleon charges will be included in the FLAG 2019 review, and hopefully more lattice nucleon quantities

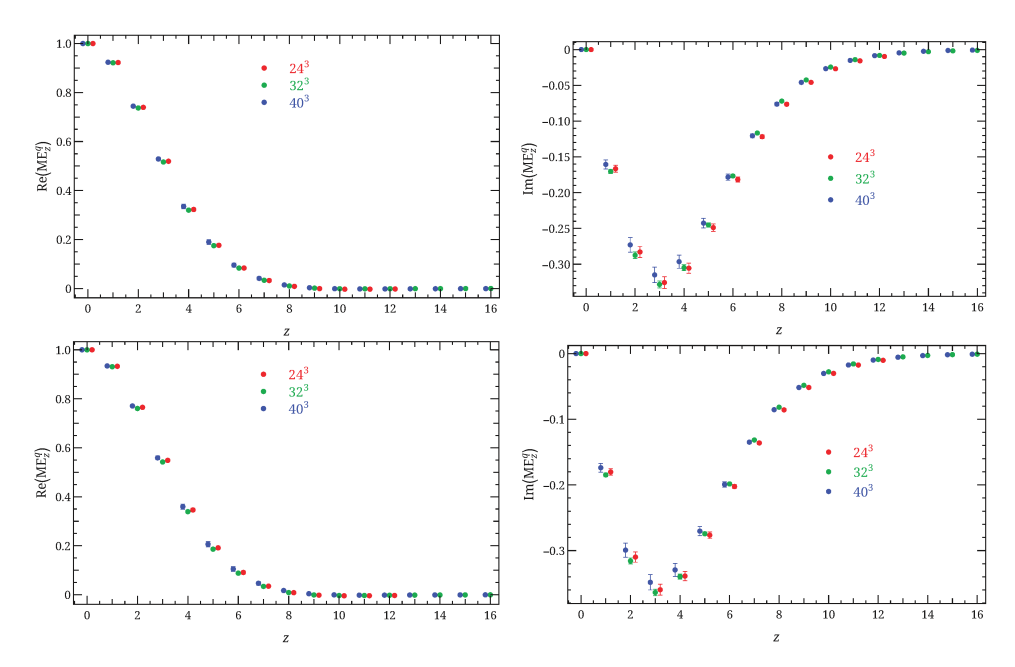


Fig. 14. (Color online) The normalized isovector nucleon matrix elements for unpolarized (top) and polarized PDFs  $P_z \approx 1.3$  GeV as functions of z at the three volumes ( $M_{\pi}L = 3.3$ , 4.4 and 5.5 indicated by red, green and blue, respectively). The matrix elements are scaled by an exponential factor  $\exp(0.15z)$  so that the large-z matrix elements can be seen more clearly.

will be included in the near future. Simultaneously, there have been rapid developments in lattice-QCD calculations of proton structure, especially in the Bjorken-x dependence of parton distribution functions (PDFs), overcoming a longstanding obstacle. For the first time, Bjorken-x dependence of many distributions been studied: nucleon gluon and isovector unpolarized, helicity and transversity distributions,  $^{19,21,169}$  the first pion and kaon distribution amplitudes,  $^{176,177}$  pion PDF  $^{178}$  and generalized parton distributions.  $^{179}$  Such studies have been giving us a first direct look into the mysteries of Bjorken-x structure. However, this work is only just beginning, and future structure calculations should be expected to achieve FLAG standards and treat all systematics properly; a few important directions are currently being pursued.

Study of Systematics Underway: The first study of the systematic uncertainties arising from finite-volume (FV) effects for the quasi-distributions was reported in Ref. 180 using 220-MeV pion mass with  $M_{\pi}^{\rm val}L \approx 3.3$ , 4.4 and 5.5, respectively. After carefully extracting the bare matrix elements for the unpolarized and polarized distributions (see Fig. 14), there is no observed volume dependence in these ensembles within the statistical error. The quasi-PDF distribution is checked again after applying NPR, and it remains consistent within statistical errors. We conclude that finite-volume dependence does not play a significant role

for the boosted nucleon matrix elements used for quasi-distributions within the range of  $M_{\pi}^{\text{val}}L \in \{3.3, 5.5\}$ .

Impact on Parton Distribution Functions: How can the current lattice-QCD isovector PDF calculations contribute to global PDF fits in the next 5 years? Currently, the large-x regions of the PDFs are not well constrained by the experimental data in the global fits, or they suffer hard-to-quantify nuclear-theory uncertainty. The lattice isovector PDFs at large x, do not have large boost-momentum dependence (unlike the small-x region), so it should be able to provide good constraints to the global PDF fit. The white paper<sup>36</sup> from the first joint-community workshop between the LQCD and global analysis communities gives an estimation of the precision needed and its corresponding impacts on the global PDF fits for the most-studied unpolarized PDF and helicity cases. Firstly, a set of pseudo-data for the isovector combinations at  $Q^2 = 4$  GeV<sup>2</sup>

$$u(x_i, Q^2) - d(x_i, Q^2)$$
 and  $\bar{u}(x_i, Q^2) - \bar{d}(x_i, Q^2)$ ,  $i = 1, \dots, N_x$ , (24)

for the unpolarized case, and

$$\Delta u(x_i, Q^2) - \Delta d(x_i, Q^2)$$
 and  $\Delta \bar{u}(x_i, Q^2) - \Delta \bar{d}(x_i, Q^2)$ ,  $i = 1, ..., N_x$ , (25)

for the polarized case, with  $N_x$  being the number of points in x-space that are being sampled. For this study, we choose the  $N_x = 5$  points taken from lattice-QCD computations to be

$$x_i \in \{0.70, 0.75, 0.80, 0.85, 0.90\}.$$
 (26)

Three scenarios for the total uncertainty of  $\delta_L^{(i)} = 12\%$ , 6% and 3% are denoted by Scenario D, E, and F, respectively. For each scenario, we assume the same relative error for each value of  $\{x_i\}$ , and we neglect possible correlations between neighboring x-points. The results of this exercise are summarized in Fig. 15, where we plot the ratio of the PDF uncertainties in each scenario to the uncertainty of the original NNPDF3.1 (NNPDFpol1.1) set. The impact on the PDF uncertainties in  $\bar{u}$  and d at large x is shown in the upper plots, with the corresponding comparison for  $\Delta \bar{u}$ and  $\Delta d$  in the lower plots. The results for the individual quark flavors shown, even though the constraints are imposed on differences between flavors, since the former are of more interest to phenomenology. From this comparison, the lattice-QCD calculations of the x-dependence of PDFs can significantly reduce the uncertainties for both unpolarized and polarized antiquarks in the large-x region. Taking into account that the PDF uncertainties on the large-x antiquarks are rather large and that they enter a number of important beyond-the-Standard Model (BSM) search channels (such as, for instance, production of new heavy gauge bosons W' and Z'), our analysis demonstrates that such calculations would have direct phenomenological implications. In a Monte-Carlo approach such as NNPDF, the PDF uncertainties themselves fluctuate, particularly at low scales, which explains the wiggles seen in these plots.

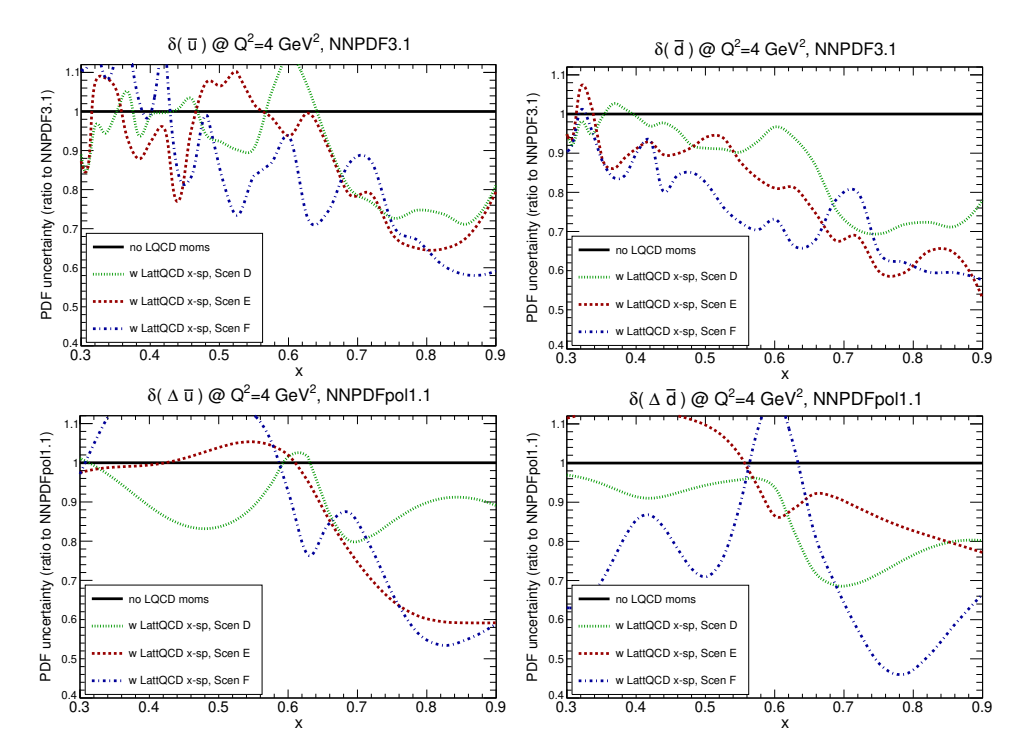


Fig. 15. The ratio of PDF uncertainties to the original NNPDF3.1 (NNPDFpol1.1) in the fits where lattice-QCD pseudo-data for x-space PDFs have been added to the global unpolarized (polarized) analysis. Specifically, we show the impact on the PDF uncertainties in  $\bar{u}$  and  $\bar{d}$  at large x in the upper plots, with the corresponding comparison for  $\Delta \bar{u}$  and  $\Delta \bar{d}$  in the lower plots. These plots are taken from Ref. 36.

Figure 15 shows that in the unpolarized case, the large-x PDF uncertainties could be reduced to 60% of their original values. It is also found that there are no large differences between the three scenarios, probably because the constraint is on quark differences rather than on individual flavors, so there is freedom for  $\bar{u}$  and  $\bar{d}$  to vary in a correlated fashion while still satisfying the constraint. However, it does suggest that a direct lattice-QCD calculation of  $x\bar{u} - x\bar{d}$  does not need to reach uncertainties at the few-percent level to influence global fits. For the polarized PDFs, Fig. 15 demonstrates that the reduction in PDF uncertainties could be significantly more marked. For instance, in the case of  $\Delta \bar{d}$ , at  $x \simeq 0.8$  the resulting PDF uncertainty from Scenario F is less than 50% of the original uncertainty.

Machine-Learning Predictions for Small-x Distributions: Even with progress made so far, there remain challenges to reliably extract small-x distributions and antiquark distributions. Figure 11 shows the recent effort<sup>181</sup> toward demonstrating the capability to reach high boost momentum in the LaMET method. One can see the reproduction of the PDF is much more sensitive to the size of  $P_z$  in the antiquark (negative x) region. Such an effect is also clearly seen in the LQCD

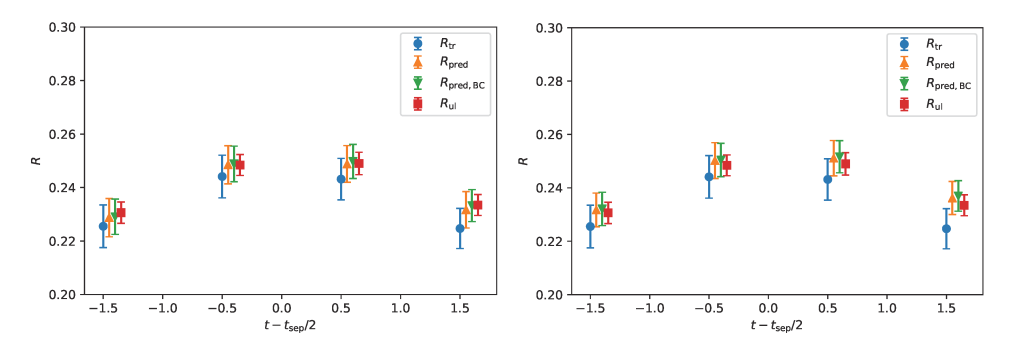


Fig. 16. (Middle row) The ratio plots of the kaon quasi-PDF correlators at  $z_{\rm pred}=4$ ,  $p_{\rm pred}=4$  from direct measurements and the predictions of the three models; from left to right they are: (1) GBT model with inputs of  $z_{\rm in}=4$ ,  $p_{\rm in}=3$  (2) same inputs as (1) but with linear model All these results are obtained using the number of estimator  $N_{\rm est}=150$ , learning rate of r=0.1 for GBT models, training and bias-correction measurements of  $N_{\rm tr}=N_{\rm BC}=240$  and  $N_{\rm ul}=1180$  are used. The calculation is done at lattice spacing 0.12 fm with pion mass of 220 MeV using clover valence fermion on HISQ lattices; the plots are taken from Ref. 181.

calculation with small  $P_z$ . References 22 and 143 study PDFs with  $P_z \leq 1.4$  GeV, and found the wrong sign of the sea flavor asymmetry. One can clearly see that such an effect is predicted by the exercise, as shown in the middle plot of Fig. 11. One can also see that as momentum increases, the reconstructed PDF recovers the smaller-x region better; therefore, it is crucial to get to larger  $P_z$  to get the antiquark PDF with the correct sign and reach smaller x. A later lattice PDF calculation, <sup>23</sup> using boost momenta up to 3 GeV, fixed the problem seen in earlier works, <sup>22,143</sup> as shown in the middle plot of Fig. 11.

However, the signal-to-noise ratio deteriorates quickly as momentum  $P_z$  increases. Using finer lattice spacings will allow us to to control discretization errors as well as having reliable matching of the quasi-PDF to the lightcone PDF. However, such calculations would be far more costly than calculations using coarse lattices at the same pion mass. Furthermore, this is not an unique issue with "quasi-PDF" or LaMET methods. Similar problems occur in the hadronic-tensor method, <sup>14,16</sup> pseudo-PDF method, <sup>131,139</sup> and lattice good cross section (LGC). To be able to reach small-x regions, say x < 0.01, all these methods require larger-momentum calculations than those being done today.

The first round of exploratory studies applying machine-learning algorithms to lattice calculations of LaMET data<sup>181</sup> demonstrated promising signs that invite further exploration of the approach. Reference 181 applied machine-learning algorithms to make predictions for different types of real lattice LaMET data, such as kaon PDFs, meson distribution amplitudes (DAs) and gluon PDFs.<sup>181</sup> The data correlation dependence on the number of training and bias-correction data, and machine-learning model parameters were studied in great detail. Figure 16 shows selected predictions from Ref. 181 with the observed datasets for both predictions of higher boost momentum (p-predictions). It is found that both algorithms can

reliably predict the target observables with different fit quality and systematic errors. The predictions from smaller displacement z to larger ones work better than those for momentum p due to the higher correlation among the data, whereas the momentum predictions depend on the precision of the available data. It would be interesting to see more studies done in this direction to make breakthrough for the small-x region of nucleon-structure studies.

# Acknowledgments

We thank the MILC Collaboration for sharing the lattices used to perform this study. The LQCD calculations were performed using the Chroma software suite. <sup>182</sup> This research used resources of the National Energy Research Scientific Computing Center, a DOE Office of Science User Facility supported by the Office of Science of the U.S. Department of Energy under Contract No. DE-AC02-05CH11231 through ALCC and ERCAP; facilities of the USQCD Collaboration, which are funded by the Office of Science of the U.S. Department of Energy, and supported in part by Michigan State University through computational resources provided by the Institute for Cyber-Enabled Research. H.-W. Lin is supported by the US National Science Foundation under grant PHY 1653405 "CAREER: Constraining Parton Distribution Functions for New-Physics Searches."

### References

- R. Gupta, Y.-C. Jang, B. Yoon, H.-W. Lin, V. Cirigliano and T. Bhattacharya, *Phys. Rev. D* 98, 034503 (2018), arXiv:1806.09006 [hep-lat].
- H.-W. Lin, J.-W. Chen, X. Ji, L. Jin, R. Li, Y.-S. Liu, Y.-B. Yang, J.-H. Zhang and Y. Zhao, *Phys. Rev. Lett.* 121, 242003 (2018), arXiv:1807.07431 [hep-lat].
- T. Bhattacharya, V. Cirigliano, S. Cohen, R. Gupta, H.-W. Lin and B. Yoon, *Phys. Rev. D* 94, 054508 (2016), arXiv:1606.07049 [hep-lat].
- PNDME Collab. (T. Bhattacharya et al.), Phys. Rev. D 92, 094511 (2015), arXiv:1506.06411 [hep-lat].
- J. R. Green, J. W. Negele, A. V. Pochinsky, S. N. Syritsyn, M. Engelhardt and S. Krieg, *Phys. Rev. D* 86, 114509 (2012), arXiv:1206.4527 [hep-lat].
- Y. Aoki, T. Blum, H.-W. Lin, S. Ohta, S. Sasaki, R. Tweedie, J. Zanotti and T. Yamazaki, Phys. Rev. D 82, 014501 (2010), arXiv:1003.3387 [hep-lat].
- A. Abdel-Rehim et al., Phys. Rev. D 92, 114513 (2015) [Erratum: ibid. 93, 039904 (2016)], arXiv:1507.04936 [hep-lat].
- G. S. Bali, S. Collins, B. Glässle, M. Göckeler, J. Najjar, R. H. Rödl, A. Schäfer, R. W. Schiel, W. Söldner and A. Sternbeck, *Phys. Rev. D* 91, 054501 (2015), arXiv:1412. 7336 [hep-lat].
- RBC+UKQCD Collab. (T. Yamazaki et al.), Phys. Rev. Lett. 100, 171602 (2008), arXiv:0801.4016 [hep-lat].
- H.-W. Lin, W. Melnitchouk, A. Prokudin, N. Sato and H. Shows, *Phys. Rev. Lett.* 120, 152502 (2018), arXiv:1710.09858 [hep-ph].
- QCDSF Collab. (M. Gockeler et al.), Phys. Rev. D 71, 114511 (2005), arXiv:hep-ph/0410187.

- Z. Davoudi and M. J. Savage, Phys. Rev. D 86, 054505 (2012), arXiv:1204.4146 [hep-lat].
- W. Detmold and C. J. D. Lin, Phys. Rev. D 73, 014501 (2006), arXiv:hep-lat/ 0507007.
- 14. K.-F. Liu and S.-J. Dong, *Phys. Rev. Lett.* **72**, 1790 (1994), arXiv:hep-ph/9306299.
- K. F. Liu, S. J. Dong, T. Draper, D. Leinweber, J. H. Sloan, W. Wilcox and R. M. Woloshyn, *Phys. Rev. D* 59, 112001 (1999), arXiv:hep-ph/9806491.
- 16. K.-F. Liu, Phys. Rev. D 62, 074501 (2000), arXiv:hep-ph/9910306.
- 17. K.-F. Liu, PoS LATTICE2015, 115 (2016), arXiv:1603.07352 [hep-ph].
- 18. X. Ji, Phys. Rev. Lett. 110, 262002 (2013), arXiv:1305.1539 [hep-ph].
- H.-W. Lin, J.-W. Chen, S. D. Cohen and X. Ji, *Phys. Rev. D* 91, 054510 (2015), arXiv:1402.1462 [hep-ph].
- C. Alexandrou, K. Cichy, V. Drach, E. Garcia-Ramos, K. Hadjiyiannakou, K. Jansen,
   F. Steffens and C. Wiese, *Phys. Rev. D* 92, 014502 (2015), arXiv:1504.07455 [hep-lat].
- J.-W. Chen, S. D. Cohen, X. Ji, H.-W. Lin and J.-H. Zhang, Nucl. Phys. B 911, 246 (2016), arXiv:1603.06664 [hep-ph].
- C. Alexandrou, K. Cichy, M. Constantinou, K. Jansen, A. Scapellato and F. Steffens, Phys. Rev. Lett. 121, 112001 (2018), arXiv:1803.02685 [hep-lat].
- J.-W. Chen, L. Jin, H.-W. Lin, Y.-S. Liu, Y.-B. Yang, J.-H. Zhang and Y. Zhao, arXiv:1803.04393 [hep-lat].
- 24. H.-W. Lin, Int. J. Mod. Phys. Conf. Ser. 25, 1460039 (2014).
- 25. H.-W. Lin, PoS LATTICE2013, 293 (2014).
- C. Alexandrou, K. Cichy, M. Constantinou, K. Hadjiyiannakou, K. Jansen, F. Steffens and C. Wiese, Phys. Rev. D 96, 014513 (2017), arXiv:1610.03689 [hep-lat].
- 27. M. Di Pierro, From Monte Carlo integration to lattice quantum chromodynamics: An Introduction, in *GSA Summer School on Physics on the Frontier and in the Future Batavia*, Illinois, 31 July–7 August 2000 (2000), arXiv:hep-lat/0009001.
- G. P. Lepage, Lattice QCD for novices, in Strong Interactions at Low and Intermediate Energies. Proc. 13th Annual Hampton University Graduate Studies, HUGS'98, Newport News, USA, 26 May-12 June 1998 (1998), pp. 49-90, arXiv:hep-lat/0506036.
- M. Luscher, Advanced lattice QCD, in Probing the Standard Model of Particle Interactions. Proc., Summer School in Theoretical Physics, NATO Advanced Study Institute, 68th session, Les Houches, France, 28 July–5 September 1997 (1998), pp. 229– 280, arXiv:hep-lat/9802029.
- R. Gupta, Introduction to lattice QCD: Course, in Probing the Standard Model of Particle Interactions. Proc., Summer School in Theoretical Physics, NATO Advanced Study Institute, 68th session, Les Houches, France, 28 July–5 September 1997 (1997), pp. 83–219, arXiv:hep-lat/9807028.
- 31. D. Landau and K. Binder, A Guide to Monte Carlo Simulations in Statistical Physics (Cambridge University Press, 2015).
- 32. M. Newman and G. Barkema, Monte Carlo Methods in Statistical Physics (Oxford University Press, 1999).
- 33. S. J. Brodsky, A. L. Deshpande, H. Gao, R. D. McKeown, C. A. Meyer, Z.-E. Meziani, R. G. Milner, J. Qiu, D. G. Richards and C. D. Roberts, arXiv:1502.05728 [hep-ph].
- 34. E.-C. Aschenauer et al., Eur. Phys. J. A 53, 71 (2017), arXiv:1410.8831 [hep-ph].
- 35. S. Aoki et al., Eur. Phys. J. C 77, 112 (2017), arXiv:1607.00299 [hep-lat].

- 36. H.-W. Lin et al., Prog. Part. Nucl. Phys. 100, 107 (2018), arXiv:1711.07916 [hep-ph].
- 37. Flavour Lattice Averaging Group Collab. (S. Aoki et al.), arXiv:1902.08191 [hep-lat].
- 38. M. Golterman, Applications of chiral perturbation theory to lattice QCD, in *Modern Perspectives in Lattice QCD: Quantum Field Theory and High Performance Computing*, 93rd Session, Les Houches, France, 3–28 August 2009 (2009), pp. 423–515, arXiv:0912.4042 [hep-lat].
- 39. A. Savanur and H.-W. Lin, arXiv:1901.00018 [hep-lat].
- 40. M. Luscher, Commun. Math. Phys. 104, 177 (1986).
- 41. M. Luscher, Commun. Math. Phys. 105, 153 (1986).
- 42. G. P. Lepage, *The Analysis of Algorithms for Lattice Field Theory*, Boulder (ASI, 1989), pp. 97–120.
- H.-W. Lin, S. D. Cohen, R. G. Edwards, K. Orginos and D. G. Richards, *PoS LAT-TICE2008*, 140 (2008), arXiv:0810.5141 [hep-lat].
- H.-W. Lin, S. D. Cohen, R. G. Edwards and D. G. Richards, *Phys. Rev. D* 78, 114508 (2008), arXiv:0803.3020 [hep-lat].
- 45. H.-W. Lin, S. D. Cohen, R. G. Edwards, K. Orginos and D. G. Richards, arXiv:1005. 0799 [hep-lat].
- T. Bhattacharya, S. D. Cohen, R. Gupta, A. Joseph, H.-W. Lin and B. Yoon, *Phys. Rev. D* 89, 094502 (2014), arXiv:1306.5435 [hep-lat].
- 47. G. Martinelli, C. Pittori, C. T. Sachrajda, M. Testa and A. Vladikas, *Nucl. Phys. B* 445, 81 (1995), arXiv:hep-lat/9411010.
- 48. M. Gockeler, R. Horsley, E.-M. Ilgenfritz, H. Perlt, P. E. L. Rakow, G. Schierholz and A. Schiller, *Phys. Rev. D* **54**, 5705 (1996), arXiv:hep-lat/9602029.
- V. Bernard, N. Kaiser, J. Kambor and U. G. Meissner, Nucl. Phys. B 388, 315 (1992).
- V. Bernard, N. Kaiser and U.-G. Meissner, Int. J. Mod. Phys. E 4, 193 (1995), arXiv:hep-ph/9501384.
- V. Bernard and U.-G. Meissner, Annu. Rev. Nucl. Part. Sci. 57, 33 (2007), arXiv:hep-ph/0611231.
- V. Bernard and U.-G. Meissner, Phys. Lett. B 639, 278 (2006), arXiv:hep-lat/ 0605010.
- 53. A. A. Khan et al., Phys. Rev. D 74, 094508 (2006), arXiv:hep-lat/0603028.
- G. Colangelo, A. Fuhrer and S. Lanz, *Phys. Rev. D* 82, 034506 (2010), arXiv:1005.
   1485 [hep-lat].
- 55. J. de Vries, R. G. E. Timmermans, E. Mereghetti and U. van Kolck, *Phys. Lett. B* **695**, 268 (2011), arXiv:1006.2304 [hep-ph].
- 56. S. Aoki et al., Eur. Phys. J. C 74, 2890 (2014), arXiv:1310.8555 [hep-lat].
- 57. G. Colangelo et al., Eur. Phys. J. C 71, 1695 (2011), arXiv:1011.4408 [hep-lat].
- H.-W. Lin, T. Blum, S. Ohta, S. Sasaki and T. Yamazaki, *Phys. Rev. D* 78, 014505 (2008), arXiv:0802.0863 [hep-lat].
- 59. A. Metz, *Phys. Lett. B* **549**, 139 (2002), arXiv:hep-ph/0209054.
- M. Anselmino, M. Boglione, U. D'Alesio, A. Kotzinian, F. Murgia, A. Prokudin and C. Turk, Phys. Rev. D 75, 054032 (2007), arXiv:hep-ph/0701006.
- M. Anselmino, M. Boglione, U. D'Alesio, A. Kotzinian, F. Murgia, A. Prokudin and S. Melis, Nucl. Phys. B (Proc. Suppl.) 191, 98 (2009), arXiv:0812.4366 [hep-ph].
- M. Anselmino, M. Boglione, U. D'Alesio, S. Melis, F. Murgia and A. Prokudin, *Phys. Rev. D* 87, 094019 (2013), arXiv:1303.3822 [hep-ph].
- Z.-B. Kang, A. Prokudin, P. Sun and F. Yuan, Phys. Rev. D 91, 071501 (2015), arXiv:1410.4877 [hep-ph].

- Z.-B. Kang, A. Prokudin, P. Sun and F. Yuan, Phys. Rev. D 93, 014009 (2016), arXiv:1505.05589 [hep-ph].
- 65. J. C. Collins, D. E. Soper and G. F. Sterman, Nucl. Phys. B 250, 199 (1985).
- A. Bacchetta, A. Courtoy and M. Radici, J. High Energy Phys. 03, 119 (2013), arXiv:1212.3568 [hep-ph].
- A. Bacchetta, A. Courtoy and M. Radici, *Phys. Rev. Lett.* 107, 012001 (2011), arXiv:1104.3855 [hep-ph].
- HERMES Collab. (A. Airapetian et al.), Phys. Lett. B 693, 11 (2010), arXiv:1006.
   4221 [hep-ex].
- COMPASS Collab. (M. Alekseev et al.), Phys. Lett. B 673, 127 (2009), arXiv:0802.
   160 [hep-ex].
- COMPASS Collab. (C. Adolph et al.), Phys. Lett. B 744, 250 (2015), arXiv:1408.
   4405 [hep-ex].
- T. Bhattacharya, V. Cirigliano, S. D. Cohen, A. Filipuzzi, M. Gonzalez-Alonso, M. L. Graesser, R. Gupta and H.-W. Lin, *Phys. Rev. D* 85, 054512 (2012), arXiv:1110.6448 [hep-ph].
- Nab Collab. (D. Pocanic et al.), Nucl. Instrum. Methods A 611, 211 (2009), arXiv:0810.0251 [nucl-ex].
- V. Cirigliano, M. Gonzalez-Alonso and M. L. Graesser, J. High Energy Phys. 02, 046 (2013), arXiv:1210.4553 [hep-ph].
- M. Gonzalez-Alonso, O. Naviliat-Cuncic and N. Severijns, *Prog. Part. Nucl. Phys.* 104, 165 (2019), arXiv:1803.08732 [hep-ph].
- ATLAS Collab. (M. Aaboud et al.), Eur. Phys. J. C 78, 401 (2018), arXiv:1706.04786 [hep-ex].
- S. Alioli, W. Dekens, M. Girard and E. Mereghetti, J. High Energy Phys. 08, 205 (2018), arXiv:1804.07407 [hep-ph].
- CMS Collab. (A. M. Sirunyan et al.), J. High Energy Phys. 06, 128 (2018), arXiv:1803.11133 [hep-ex].
- CMS Collab. (A. M. Sirunyan et al.), J. High Energy Phys. 06, 120 (2018), arXiv:1803.06292 [hep-ex].
- 79. Particle Data Group (M. Tanabashi et al.), Phys. Rev. D 98, 030001 (2018).
- MILC Collab. (A. Bazavov et al.), Phys. Rev. D 87, 054505 (2013), arXiv:1212.4768 [hep-lat].
- 81. A. Bazavov et al., Phys. Rev. D 98, 074512 (2018), arXiv:1712.09262 [hep-lat].
- V. Bernard, L. Elouadrhiri and U.-G. Meissner, J. Phys. G 28, R1 (2002), arXiv:hep-ph/0107088.
- MiniBooNE Collab. (A. A. Aguilar-Arevalo et al.), Phys. Rev. D 81, 092005 (2010), arXiv:1002.2680 [hep-ex].
- A. S. Meyer, M. Betancourt, R. Gran and R. J. Hill, Phys. Rev. D 93, 113015 (2016), arXiv:1603.03048 [hep-ph].
- 85. J. Morfín, Past and future of  $\nu/\bar{\nu}$  deuterium/hydrogen experiments, talk at INT Seattle, June, 2018.
- R. J. Hill, P. Kammel, W. J. Marciano and A. Sirlin, Rep. Prog. Phys. 81, 096301 (2018), arXiv:1708.08462 [hep-ph].
- S. Capitani, M. Della Morte, D. Djukanovic, G. M. von Hippel, J. Hua, B. Jäger,
   P. M. Junnarkar, H. B. Meyer, T. D. Rae and H. Wittig, *Int. J. Mod. Phys. A* 34, 1950009 (2019), arXiv:1705.06186 [hep-lat].
- C. Alexandrou, M. Constantinou, K. Hadjiyiannakou, K. Jansen, C. Kallidonis, G. Koutsou and A. Vaquero Aviles-Casco, *Phys. Rev. D* 96, 054507 (2017), arXiv:1705.03399 [hep-lat].

- 89. G. S. Bali, S. Collins, M. Gruber, A. Schäfer, P. Wein and T. Wurm, *Phys. Lett. B* **789**, 666 (2019), arXiv:1810.05569 [hep-lat].
- N. Hasan, J. Green, S. Meinel, M. Engelhardt, S. Krieg, J. Negele, A. Pochinsky and S. Syritsyn, Phys. Rev. D 97, 034504 (2018), arXiv:1711.11385 [hep-lat].
- 91. E. Shintani, K.-I. Ishikawa, Y. Kuramashi, S. Sasaki and T. Yamazaki, *Phys. Rev. D* **99**, 014510 (2019), arXiv:1811.07292 [hep-lat].
- R. Gupta, Y.-C. Jang, H.-W. Lin, B. Yoon and T. Bhattacharya, *Phys. Rev. D* 96, 114503 (2017), arXiv:1705.06834 [hep-lat].
- A. Bodek, S. Avvakumov, R. Bradford and H. S. Budd, Eur. Phys. J. C 53, 349 (2008), arXiv:0708.1946 [hep-ex].
- C. Alexandrou, S. Bacchio, M. Constantinou, J. Finkenrath, K. Hadjiyiannakou, K. Jansen, G. Koutsou and A. Vaquero Avilés-Casco, *Phys. Rev. D* 100, 014509 (2019), arXiv:1812.10311 [hep-lat].
- J. R. Green, J. W. Negele, A. V. Pochinsky, S. N. Syritsyn, M. Engelhardt and S. Krieg, *Phys. Rev. D* 90, 074507 (2014), arXiv:1404.4029 [hep-lat].
- PNDME Collab. (Y.-C. Jang, T. Bhattacharya, R. Gupta, H.-W. Lin and B. Yoon), PoS LATTICE2018, 123 (2018), arXiv:1901.00060 [hep-lat].
- 97. A. L. Fitzpatrick, W. Haxton, E. Katz, N. Lubbers and Y. Xu, arXiv:1211.2818 [hep-ph].
- 98. R. J. Hill and M. P. Solon, *Phys. Rev. D* **91**, 043505 (2015), arXiv:1409.8290 [hep-ph].
- H.-W. Lin, R. Gupta, B. Yoon, Y.-C. Jang and T. Bhattacharya, *Phys. Rev. D* 98, 094512 (2018), arXiv:1806.10604 [hep-lat].
- S. Collins, G. Bali and A. Schäfer, PoS LATTICE2007, 141 (2007), arXiv:0709.3217 [hep-lat].
- G. S. Bali, S. Collins and A. Schäfer, Comput. Phys. Commun. 181, 1570 (2010), arXiv:0910.3970 [hep-lat].
- C. Thron, S. J. Dong, K. F. Liu and H. P. Ying, Phys. Rev. D 57, 1642 (1998), arXiv:hep-lat/9707001.
- UKQCD Collab. (C. Michael, M. S. Foster and C. McNeile), Nucl. Phys. B (Proc. Suppl.) 83, 185 (2000), arXiv:hep-lat/9909036.
- T. Blum, T. Izubuchi and E. Shintani, Phys. Rev. D 88, 094503 (2013), arXiv:1208.
   4349 [hep-lat].
- T. Bhattacharya, V. Cirigliano, R. Gupta, H.-W. Lin and B. Yoon, *Phys. Rev. Lett.* 115, 212002 (2015), arXiv:1506.04196 [hep-lat].
- C. Alexandrou, M. Constantinou, K. Hadjiyiannakou, K. Jansen, C. Kallidonis,
   G. Koutsou, A. Vaquero Avilés-Casco and C. Wiese, *Phys. Rev. Lett.* 119, 142002 (2017), arXiv:1706.02973 [hep-lat].
- C. Alexandrou, M. Constantinou, K. Hadjiyiannakou, K. Jansen, C. Kallidonis,
   G. Koutsou and A. V. Avilés-Casco, EPJ Web Conf. 175, 06003 (2018), arXiv:1807.
   11203 [hep-lat].
- COMPASS Collab. (C. Adolph et al.), Phys. Lett. B 753, 18 (2016), arXiv:1503. 08935 [hep-ex].
- NNPDF Collab. (E. R. Nocera, R. D. Ball, S. Forte, G. Ridolfi and J. Rojo), Nucl. Phys. B 887, 276 (2014), arXiv:1406.5539 [hep-ph].
- D. de Florian, R. Sassot, M. Stratmann and W. Vogelsang, *Phys. Rev. Lett.* 101, 072001 (2008), arXiv:0804.0422 [hep-ph].
- D. de Florian, R. Sassot, M. Stratmann and W. Vogelsang, *Phys. Rev. D* 80, 034030 (2009), arXiv:0904.3821 [hep-ph].

- Jefferson Lab Angular Momentum Collab. (N. Sato, W. Melnitchouk, S. E. Kuhn, J. J. Ethier and A. Accardi), Phys. Rev. D 93, 074005 (2016), arXiv:1601.07782 [hep-ph].
- J. J. Ethier, N. Sato and W. Melnitchouk, Phys. Rev. Lett. 119, 132001 (2017), arXiv:1705.05889 [hep-ph].
- J. Engel, M. J. Ramsey-Musolf and U. van Kolck, *Prog. Part. Nucl. Phys.* 71, 21 (2013), arXiv:1303.2371 [nucl-th].
- 115. M. Pospelov and A. Ritz, Ann. Phys. 318, 119 (2005), arXiv:hep-ph/0504231.
- 116. J. R. Ellis and R. A. Flores, *Phys. Lett. B* **377**, 83 (1996), arXiv:hep-ph/9602211.
- T. Bhattacharya, V. Cirigliano and R. Gupta, PoS LATTICE2012, 179 (2012), arXiv:1212.4918 [hep-lat].
- R. Gupta, B. Yoon, T. Bhattacharya, V. Cirigliano, Y.-C. Jang and H.-W. Lin, *Phys. Rev. D* 98, 091501 (2018), arXiv:1808.07597 [hep-lat].
- C. A. Baker et al., Phys. Rev. Lett. 97, 131801 (2006), arXiv:hep-ex/0602020.
- N. Arkani-Hamed and S. Dimopoulos, *J. High Energy Phys.* **06**, 073 (2005), arXiv:hep-th/0405159.
- G. F. Giudice and A. Romanino, Nucl. Phys. B 699, 65 (2004) [Erratum: ibid. 706, 487 (2005)], arXiv:hep-ph/0406088.
- 122. N. Arkani-Hamed, S. Dimopoulos, G. F. Giudice and A. Romanino, *Nucl. Phys. B* 709, 3 (2005), arXiv:hep-ph/0409232.
- G. F. Giudice and A. Romanino, Phys. Lett. B 634, 307 (2006), arXiv:hep-ph/ 0510197.
- 124. ACME Collab. (V. Andreev et al.), Nature **562**, 355 (2018).
- 125. ACME Collab. (J. Baron *et al.*), *Science* **343**, 269 (2014), arXiv:1310.7534 [physics.atom-ph].
- CMS Collab. (A. M. Sirunyan et al.), J. High Energy Phys. 05, 025 (2018), arXiv:1802.02110 [hep-ex].
- 127. X. Ji, Sci. China Phys. Mech. Astron. 57, 1407 (2014), arXiv:1404.6680 [hep-ph].
- B. L. Ioffe, Phys. Lett. B 30, 123 (1969).
- V. Braun, P. Gornicki and L. Mankiewicz, Phys. Rev. D 51, 6036 (1995), arXiv:hep-ph/9410318.
- 130. A. Radyushkin, *Phys. Lett. B* **767**, 314 (2017), arXiv:1612.05170 [hep-ph].
- 131. A. V. Radyushkin, *Phys. Rev. D* **96**, 034025 (2017), arXiv:1705.01488 [hep-ph].
- 132. Y.-Q. Ma and J.-W. Qiu, *Phys. Rev. D* 98, 074021 (2018), arXiv:1404.6860 [hep-ph].
- Y.-Q. Ma and J.-W. Qiu, Int. J. Mod. Phys. Conf. Ser. 37, 1560041 (2015), arXiv:1412.2688 [hep-ph].
- U. Aglietti, M. Ciuchini, G. Corbo, E. Franco, G. Martinelli and L. Silvestrini, *Phys. Lett. B* 432, 411 (1998), arXiv:hep-ph/9804416.
- J. Liang, K.-F. Liu and Y.-B. Yang, EPJ Web Conf. 175, 14014 (2018), arXiv:1710.
   11145 [hep-lat].
- W. Detmold, I. Kanamori, C. J. D. Lin, S. Mondal and Y. Zhao, PoS LAT-TICE2018, 106 (2018), arXiv:1810.12194 [hep-lat].
- A. J. Chambers, R. Horsley, Y. Nakamura, H. Perlt, P. E. L. Rakow, G. Schierholz,
   A. Schiller, K. Somfleth, R. D. Young and J. M. Zanotti, *Phys. Rev. Lett.* 118, 242001 (2017), arXiv:1703.01153 [hep-lat].
- X. Xiong, X. Ji, J.-H. Zhang and Y. Zhao, Phys. Rev. D 90, 014051 (2014), arXiv:1310.7471 [hep-ph].
- K. Orginos, A. Radyushkin, J. Karpie and S. Zafeiropoulos, *Phys. Rev. D* 96, 094503 (2017), arXiv:1706.05373 [hep-ph].

- C. Monahan and K. Orginos, J. High Energy Phys. 03, 116 (2017), arXiv:1612.01584 [hep-lat].
- J.-W. Chen, T. Ishikawa, L. Jin, H.-W. Lin, Y.-B. Yang, J.-H. Zhang and Y. Zhao, Phys. Rev. D 97, 014505 (2018), arXiv:1706.01295 [hep-lat].
- J. Green, K. Jansen and F. Steffens, Phys. Rev. Lett. 121, 022004 (2018), arXiv:1707.
   07152 [hep-lat].
- 143. LP3 Collab. (H.-W. Lin, J.-W. Chen, T. Ishikawa and J.-H. Zhang), Phys. Rev. D 98, 054504 (2018), arXiv:1708.05301 [hep-lat].
- Y.-S. Liu, J.-W. Chen, L. Jin, R. Li, H.-W. Lin, Y.-B. Yang, J.-H. Zhang and Y. Zhao, arXiv:1810.05043 [hep-lat].
- C. Alexandrou, K. Cichy, M. Constantinou, K. Jansen, A. Scapellato and F. Steffens, Phys. Rev. D 98, 091503 (2018), arXiv:1807.00232 [hep-lat].
- C. Alexandrou, K. Cichy, M. Constantinou, K. Hadjiyiannakou, K. Jansen,
   A. Scapellato and F. Steffens, *Phys. Rev. D* 99, 114504 (2019), arXiv:1902.00587
   [hep-lat].
- T. Izubuchi, X. Ji, L. Jin, I. W. Stewart and Y. Zhao, *Phys. Rev. D* 98, 056004 (2018), arXiv:1801.03917 [hep-ph].
- W. Wang, S. Zhao and R. Zhu, Eur. Phys. J. C 78, 147 (2018), arXiv:1708.02458 [hep-ph].
- 149. W. Wang and S. Zhao, J. High Energy Phys. 05, 142 (2018), arXiv:1712.09247 [hep-ph].
- X. Ji, J.-H. Zhang and Y. Zhao, Phys. Rev. Lett. 120, 112001 (2018), arXiv:1706. 08962 [hep-ph].
- T. Ishikawa, Y.-Q. Ma, J.-W. Qiu and S. Yoshida, Phys. Rev. D 96, 094019 (2017), arXiv:1707.03107 [hep-ph].
- C. Alexandrou, K. Cichy, M. Constantinou, K. Hadjiyiannakou, K. Jansen,
   H. Panagopoulos and F. Steffens, Nucl. Phys. B 923, 394 (2017), arXiv:1706.00265
   [hep-lat].
- M. Constantinou and H. Panagopoulos, Phys. Rev. D 96, 054506 (2017), arXiv:1705.
   11193 [hep-lat].
- 154. X. Xiong, T. Luu and U.-G. Meißner, arXiv:1705.00246 [hep-ph].
- J.-W. Chen, X. Ji and J.-H. Zhang, Nucl. Phys. B 915, 1 (2017), arXiv:1609.08102
   [hep-ph].
- 156. T. Ishikawa, Y.-Q. Ma, J.-W. Qiu and S. Yoshida, arXiv:1609.02018 [hep-lat].
- HPQCD and UKQCD Collabs. (E. Follana et al.), Phys. Rev. D 75, 054502 (2007), arXiv:hep-lat/0610092.
- G. S. Bali, B. Lang, B. U. Musch and A. Schäfer, Phys. Rev. D 93, 094515 (2016), arXiv:1602.05525 [hep-lat].
- 159. Y.-S. Liu *et al.*, arXiv:1807.06566 [hep-lat].
- S. Dulat, T.-J. Hou, J. Gao, M. Guzzi, J. Huston, P. Nadolsky, J. Pumplin,
   C. Schmidt, D. Stump and C. P. Yuan, *Phys. Rev. D* 93, 033006 (2016), arXiv:1506.
   07443 [hep-ph].
- T. Ishikawa, L. Jin, H.-W. Lin, A. Schäfer, Y.-B. Yang, J.-H. Zhang and Y. Zhao, Sci. China Phys. Mech. Astron. 62, 991021 (2019), arXiv:1711.07858 [hep-ph].
- J. Karpie, K. Orginos, A. Rothkopf and S. Zafeiropoulos, J. High Energy Phys. 04, 057 (2019), arXiv:1901.05408 [hep-lat].
- NNPDF Collab. (R. D. Ball et al.), Eur. Phys. J. C 77, 663 (2017), arXiv:1706.00428 [hep-ph].
- A. Accardi, L. T. Brady, W. Melnitchouk, J. F. Owens and N. Sato, *Phys. Rev. D* 93, 114017 (2016), arXiv:1602.03154 [hep-ph].

- QCDSF and UKQCD Collabs. (R. Horsley et al.), Phys. Lett. B 714, 312 (2012), arXiv:1205.6410 [hep-lat].
- 166. M. Deka et al., Phys. Rev. D 91, 014505 (2015), arXiv:1312.4816 [hep-lat].
- C. Alexandrou, M. Constantinou, K. Hadjiyiannakou, K. Jansen, H. Panagopoulos and C. Wiese, *Phys. Rev. D* 96, 054503 (2017), arXiv:1611.06901 [hep-lat].
- Y.-B. Yang, M. Gong, J. Liang, H.-W. Lin, K.-F. Liu, D. Pefkou and P. Shanahan, Phys. Rev. D 98, 074506 (2018), arXiv:1805.00531 [hep-lat].
- Z.-Y. Fan, Y.-B. Yang, A. Anthony, H.-W. Lin and K.-F. Liu, *Phys. Rev. Lett.* 121, 242001 (2018), arXiv:1808.02077 [hep-lat].
- Y.-Q. Ma and J.-W. Qiu, Phys. Rev. Lett. 120, 022003 (2018), arXiv:1709.03018 [hep-ph].
- 171. Y.-B. Yang, M. Glatzmaier, K.-F. Liu and Y. Zhao, arXiv:1612.02855 [nucl-th].
- 172. J. Butterworth et al., J. Phys. G 43, 023001 (2016), arXiv:1510.03865 [hep-ph].
- 173. I. Balitsky, W. Morris and A. Radyushkin, arXiv:1910.13963 [hep-ph].
- 174. W. Wang, J.-H. Zhang, S. Zhao and R. Zhu, Phys. Rev. D 100, 074509 (2019), arXiv:1904.00978 [hep-ph].
- J.-H. Zhang, X. Ji, A. Schäfer, W. Wang and S. Zhao, *Phys. Rev. Lett.* 122, 142001 (2019), arXiv:1808.10824 [hep-ph].
- J.-H. Zhang, J.-W. Chen, X. Ji, L. Jin and H.-W. Lin, *Phys. Rev. D* 95, 094514 (2017), arXiv:1702.00008 [hep-lat].
- LP3 Collab. (J.-H. Zhang et al.), Nucl. Phys. B 939, 429 (2019), arXiv:1712.10025 [hep-ph].
- 178. J.-H. Zhang, J.-W. Chen, L. Jin, H.-W. Lin, A. Schäfer and Y. Zhao, *Phys. Rev. D* 100, 034505 (2019), arXiv:1804.01483 [hep-lat].
- 179. J.-W. Chen, H.-W. Lin and J.-H. Zhang, arXiv:1904.12376 [hep-lat].
- 180. H.-W. Lin and R. Zhang, Phys. Rev. D 100, 074502 (2019).
- 181. R. Zhang, Z. Fan, R. Li, H.-W. Lin and B. Yoon, arXiv:1909.10990 [hep-lat].
- 182. SciDAC, LHPC and UKQCD Collabs. (R. G. Edwards and B. Joo), *Nucl. Phys. B* (*Proc. Suppl.*) **140**, 832 (2005), arXiv:hep-lat/0409003.